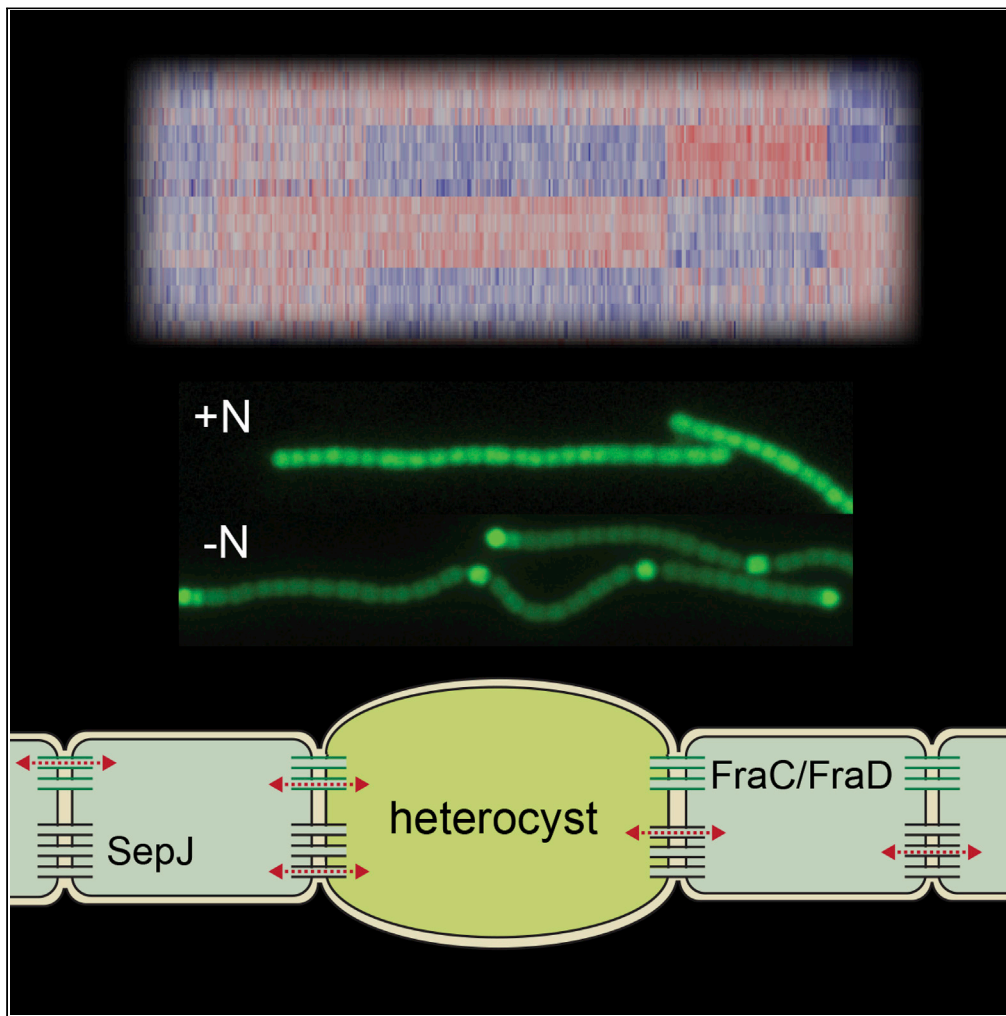# iScience

Article

Impaired cell-cell communication in the multicellular cyanobacterium *Anabaena* affects carbon uptake, photosynthesis, and the cell wall

Sergio Camargo, Dena Leshkowitz, Bareket Dassa, Vicente Mariscal, Enrique Flores, Joel Stavans, Rinat Arbel-Goren

eflores@ibvf.csic.es (E.F.)
joel.stavans@weizmann.ac.il (J.S.)

Highlights

SepJ and Fra septal proteins are key for communication in *Anabaena* filaments

Spatial expression of a regulatory gene is affected when those proteins are missing

The transcriptomes of *Anabaena* wild-type and septal protein mutants were mapped

Deletion of those proteins leads to global and specific changes in gene expression

iScience

Article

Impaired cell-cell communication in the multicellular cyanobacterium *Anabaena* affects carbon uptake, photosynthesis, and the cell wall

Sergio Camargo,[1] Dena Leshkowitz,[2] Bareket Dassa,[2] Vicente Mariscal,[3] Enrique Flores,[3,*] Joel Stavans,[1,4,*] and Rinat Arbel-Goren[1]

Summary

Cell-cell communication is an essential attribute of multicellular organisms. The effects of perturbed communication were studied in septal protein mutants of the heterocyst-forming filamentous cyanobacterium *Anabaena* sp. PCC 7120 model organism. Strains bearing *sepJ* and *sepJ/fraC/fraD* deletions showed differences in growth, pigment absorption spectra, and spatial patterns of expression of the *hetR* gene encoding a heterocyst differentiation master regulator. Global changes in gene expression resulting from deletion of those genes were mapped by RNA sequencing analysis of wild-type and mutant strains, both under nitrogen-replete and nitrogen-poor conditions. The effects of *sepJ* and *fraC/fraD* deletions were non-additive, and perturbed cell-cell communication led to significant changes in global gene expression. Most significant effects, related to carbon metabolism, included increased expression of genes encoding carbon uptake systems and components of the photosynthetic apparatus, as well as decreased expression of genes encoding cell wall components related to heterocyst differentiation and to polysaccharide export.

Introduction

Multicellularity in an organism is predicated on the molecular transfer of metabolites, nutrients, and signals that enables communication between its cells, division of labor, and cooperation (Herrero et al., 2016). Due to the many evolutionary advantages it confers, multicellularity arose independently and in many contexts other than metazoans or plants, such as in slime molds, ciliates, and prokaryotes (Lyons and Kolter, 2015). One of the earliest examples of multicellularity is furnished by filamentous cyanobacteria such as *Anabaena* sp. strain PCC 7120 (hereafter *Anabaena*) (Herrero et al., 2016). The basic structure of an *Anabaena* filament consists of a one-dimensional array of cells (Herrero et al., 2016; Flores et al., 2018), each delimited by a cytoplasmic membrane surrounded by a peptidoglycan mesh. An outer membrane spans the entire filament, defining a continuous periplasmic space (Mariscal et al., 2007; Wilk et al., 2011). Filament integrity is maintained by both cell wall components, the outer membrane and the peptidoglycan mesh (Burnat et al., 2014). Septal junctions, which likely traverse the septal peptidoglycan through nanopores, join adjacent cells and facilitate cell-cell communication (Flores et al., 2018). Furthermore, septal junction-related proteins are important for filament integrity (Flores et al., 2007; Nayar et al., 2007; Merino-Puerto et al., 2010).

Under nitrogen-replete conditions, all cells in an *Anabaena* filament carry out both photosynthesis and nitrogen assimilation from combined nitrogen sources. Such a filament grows by the division of each and every cell along its length into two daughter cells. However, when combined nitrogen sources become scarce, some cells along a filament differentiate into heterocysts, micro-oxic cells specialized in atmospheric nitrogen fixation. The differentiation of a vegetative cell into a heterocyst involves large morphological and metabolic changes that are controlled by a specific program of gene expression (Flores et al., 2019). This program is orchestrated by two main regulators: the global transcription factor NtcA and the differentiation-specific factor HetR (Herrero et al., 2016; Flores et al., 2019). Heterocysts supply neighboring vegetative cells with products of nitrogen fixation, e.g., glutamine and β-aspartyl-arginine dipeptide, whereas vegetative cells supply heterocysts with reduced carbon compounds, such as glutamate, alanine, and sucrose (Herrero et al., 2016). Individual heterocysts are separated by intervals of about 10–15

[1]Department of Physics of Complex Systems, Weizmann Institute of Science, Rehovot 76100, Israel

[2]Department of Life Sciences Core Facilities, Weizmann Institute of Science, Rehovot 76100, Israel

[3]Instituto de Bioquímica Vegetal y Fotosíntesis, CSIC and Universidad de Sevilla, Américo Vespucio 49, 41092 Sevilla, Spain

[4]Lead contact

*Correspondence:
eflores@ibvf.csic.es (E.F.),
joel.stavans@weizmann.ac.il (J.S.)
https://doi.org/10.1016/j.isci.2020.101977

vegetative cells where photosynthesis takes place, forming thus quasi-regular developmental patterns. Heterocysts lose the ability to divide, and developed filaments grow by division of vegetative cells. When the vegetative cell interval between two heterocysts becomes large enough, a new intercalary heterocyst grows in its midst, thereby preserving an intrinsic pattern scale. How are the development and behavior of *Anabaena* filaments affected when cell-cell communication is impaired is the overarching question we address in the present work.

Previous studies have addressed this question by inactivation of genes encoding proteins involved in the formation of septal junctions between adjacent cells. It has been proposed that septal junctions are at least of two types (Merino-Puerto et al., 2011), comprising the septal proteins SepJ, FraC, and FraD (Mullineaux et al., 2008; Merino-Puerto et al., 2010, 2011; Mariscal et al., 2011; Ramos-León et al., 2018). Inactivation of the *sepJ* gene results in slow intercellular molecular transfer of calcein (Mullineaux et al., 2008; Mariscal et al., 2011), and SepJ has been implicated in the transfer of an inhibitory morphogen that impedes the formation of contiguous heterocysts (Rivers et al., 2014; Corrales-Guerrero et al., 2015). FraC and FraD have been suggested to be involved in the transfer of nutrients such as sucrose between cells (Nürnberg et al., 2015). FraC and FraD are thought to work together (Merino-Puerto et al., 2011) and indeed have been shown to be associated with the septal junctions that have been visualized by electron cryotomography (Weiss et al., 2019). Interestingly, whereas Δ*sepJ* mutants are arrested at an early stage of heterocyst differentiation upon nitrogen deprivation (Flores et al., 2007; Nayar et al., 2007), Δ*fraC*/Δ*fraD* mutants form heterocysts that are active while presenting lower nitrogenase activity than the wild-type strain (Merino-Puerto et al., 2010, 2011). Neither the Δ*sepJ* mutant nor the Δ*fraC*/Δ*fraD* mutant can grow diazotrophically.

These findings led us to enquire about the behavior of filaments in which cell-cell communication is perturbed further, by studying the characteristics of a triple mutant of *Anabaena* with a Δ*sepJ*Δ*fraC*Δ*fraD* genetic background. Previous studies have shown that under nitrogen-poor conditions, Δ*sepJ*Δ*fraC*Δ*fraD* mutant filaments display a marked fragmentation phenotype upon nitrogen deprivation (Nürnberg et al., 2015). In addition to exhibiting an altered septum structure with thinner septa and a denser peptidoglycan layer, strain Δ*sepJ*Δ*fraC*Δ*fraD* is characterized by an impaired intercellular diffusion of small fluorescent molecules and a reduction in the frequency of nanopores in intercellular septal cross walls (Nürnberg et al., 2015). As its parental *sepJ* mutant strain, the Δ*sepJ*Δ*fraC*Δ*fraD* mutant cannot form heterocysts under nitrogen-deprived conditions and cannot grow diazotrophically.

In an attempt to understand better the extent to which the addition of the Δ*fraC*/Δ*fraD* deletions to the Δ*sepJ* genetic background perturbs further the physiology of *Anabaena*, we endeavored to tease apart the differences in behavior between the Δ*sepJ* and Δ*sepJ*Δ*fraC*Δ*fraD* mutant filaments, both under nitrogen-replete and -poor conditions. Using single-cell, time-lapse microscopy, we characterized developmental spatial patterns of expression from the *hetR* promoter and autofluorescence in *Anabaena* strains with wild-type (WT), Δ*sepJ*, and Δ*sepJ*Δ*fraC*Δ*fraD* genotypes, both under nitrogen-replete and -poor conditions, and measured their cell growth and absorption spectra. To shed light on the observed behavior, we studied the differences between the transcriptomes of these strains using RNA sequencing (RNA-seq) methods (Transparent Methods). We found that perturbations to cell-cell communication in this model organism led to significant changes in expression of genes encoding specific metabolic pathways as well as various cellular structures.

Results

Contrasting patterns of *hetR* expression in septal junction mutant backgrounds under nitrogen-replete and -poor conditions

To pinpoint the differences in behavior between *Anabaena* strains with Δ*sepJ* and Δ*sepJ*Δ*fraC*Δ*fraD* genotypes, we focused on the expression of the master regulator of development *hetR* and characterized statistically patterns of expression from its promoter in strains bearing a P*hetR*-*gfp* reporter fusion and the autofluorescence of photosynthetic pigments. We show in Figure 1 phase contrast, GFP fluorescence, and autofluorescence images of filaments of strains carrying the P*hetR*-*gfp* construct in WT, Δ*sepJ*, and Δ*sepJ*Δ*fraC*Δ*fraD* genetic backgrounds, just immediately (0 h) and 18 h after nitrogen deprivation. At this time, the filament with the WT background displayed well-defined heterocysts, as evidenced by a high GFP fluorescence intensity, low autofluorescence, and large size as in previous studies (Di Patti et al., 2018). In contrast, neither Δ*sepJ* nor Δ*sepJ*Δ*fraC*Δ*fraD* mutant background filaments exhibited heterocysts, but GFP fluorescence intensity was significantly larger in clusters of contiguous cells. The autofluorescence intensity in
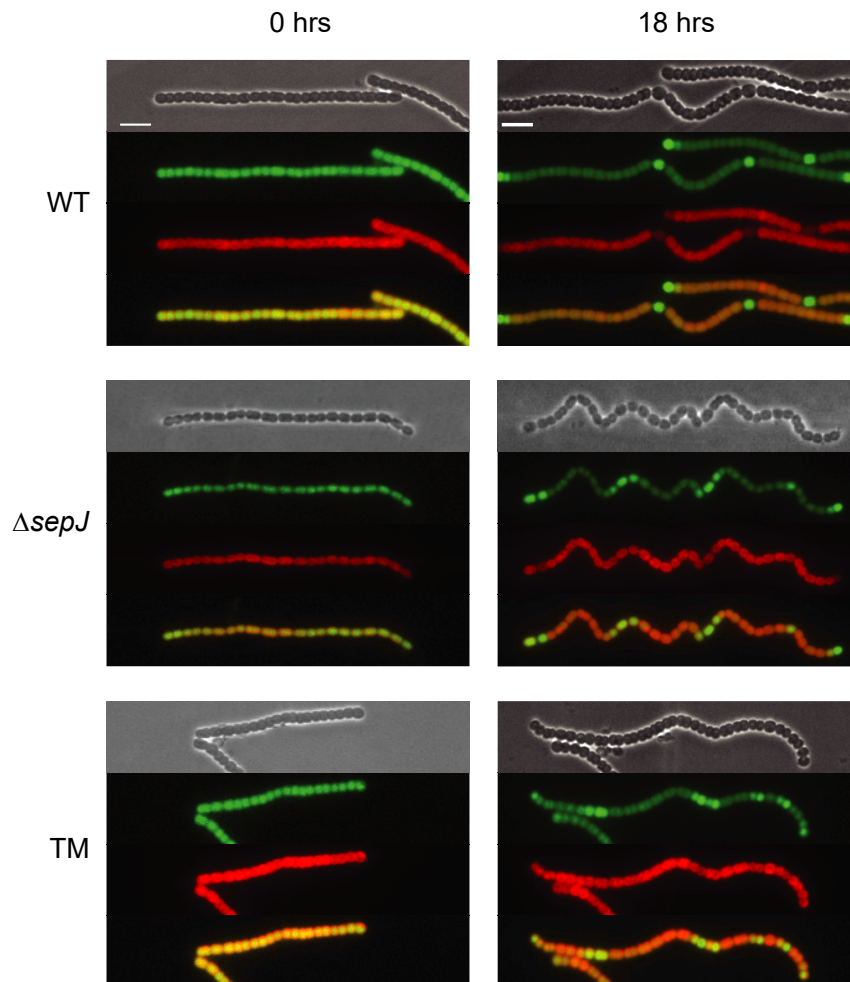
0 hrs   18 hrs

Figure 1. Behavior of septal protein deletion mutant filaments under nitrogen-replete and -poor conditions
Phase contrast, fluorescence intensity from P$_{hetR}$-gfp expression (green), autofluorescence from photosynthetic pigments (red), and their overlay, for strains carrying the P$_{hetR}$-gfp fusion in WT, ΔsepJ, and ΔsepJΔfraCΔfraD (TM) genetic backgrounds, at 0 and 18 h after nitrogen deprivation. Scale bar, 10 μM.

these cell clusters was negatively correlated with the fluorescence intensity from the P$_{hetR}$-gfp reporter fusion, consistent with the known loss of autofluorescence in cells that start differentiation. Hence, heterocyst differentiations starts in sepJ mutants as previously reported (Flores et al., 2007; Nayar et al., 2007).

However, the autofluorescence of ΔsepJ cells was visibly lower than the autofluorescence of the WT cells, whereas that of the ΔsepJΔfraCΔfraD cells was higher. This observation is captured quantitatively in Figure 2A, where we show the mean autofluorescence intensity in cells of both ΔsepJ and ΔsepJΔfraCΔfraD mutant backgrounds relative to WT background values, both immediately (0 h) and 18 h after nitrogen deprivation. To investigate this behavior further, we measured UV-visible absorption spectra of cultures (Figure 2B). Consistent with the autofluorescence results presented above, absorption spectra profiles displayed the same trends. The spectrum of the ΔsepJΔfraCΔfraD mutant background was higher than that of the WT background in the presence of nitrate for almost all the spectral range, whereas the spectrum of the ΔsepJ background was somewhat lower, particularly in the region where chlorophyll a (Chl) absorbs blue light, around 440 nm. The same trends were maintained under nitrogen deprivation, but with some differences in magnitude. After 18 h nitrogen deprivation, the differences between the spectra of the ΔsepJΔfraCΔfraD and WT backgrounds were larger mainly in the regions of Chl (centered at 440 and 680 nm), whereas the differences between the spectra of the ΔsepJ and WT backgrounds were more significant
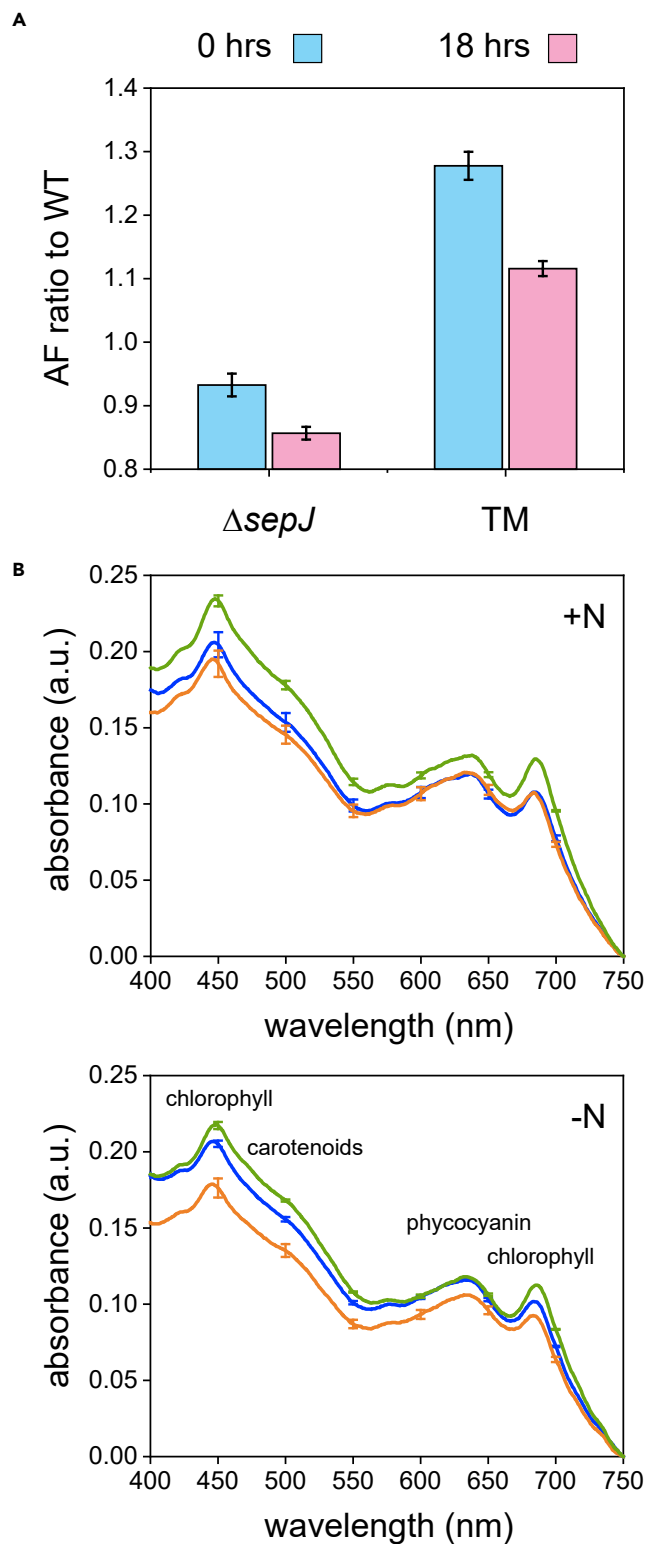
Figure 2. Differences in the behavior of the autofluorescence between strains with ΔsepJ and ΔsepJΔfraCΔfraD genetic backgrounds

(A) Mean autofluorescence intensity from photosynthetic pigments in ΔsepJ and ΔsepJΔfraCΔfraD (TM) cells normalized by the mean in WT cells measured from microscope images. Autofluorescence intensity ratios were measured at 0 h (pink)

Figure 2. *Continued*

and 18 h (cyan) after nitrogen deprivation. For each strain, mean autofluorescence intensity was measured as indicated in the Transparent Methods, from more than 500 cells in 20 filaments. Error bars denote standard errors of two independent experiments, with at least two replicates each.

(B) Absorption spectra of intact cells in WT (blue), ΔsepJ (orange), and ΔsepJΔfraCΔfraD (green) cultures in the presence of nitrate (top panel) and 18 h after nitrogen deprivation (bottom panel). For each strain, absorption spectra were measured as indicated in the Transparent Methods from two independent experiments with three replicates each.Error bars denote the corresponding standard errors. Exponentially growing cultures were adjusted to $OD_{750} = 0.4$ in growth medium.

in the phycocyanin region from 550 to 650 nm. These results suggest that the two septal junction mutants respond differently to nitrogen deprivation, and hence to the carbon-to-nitrogen balance that is key in the physiology of *Anabaena* (Herrero and Flores, 2019).

We also characterized how deletion of septal proteins affected filament growth under nitrogen-replete conditions. As absorption spectra varied between the three strains, we did not use total Chl concentration for the measurement of growth. Instead, we determined the number of cells in given filament segments directly as a function of time from our microscope observations and calculated the cell doubling time. We obtained 24 ± 2 h for the WT (similar to a value reported for liquid cultures, Pernil et al., 2008) and 36 ± 1 h and 38 ± 3 h for the ΔsepJ and ΔsepJΔfraCΔfraD backgrounds, respectively, indicating that the main difference in growth was between WT filaments on one hand and the septal mutant backgrounds ΔsepJ and ΔsepJΔfraCΔfraD on the other. Therefore, the sepJ deletion, common to both, seems to be especially responsible for the decrease in growth rate.

To characterize the statistical differences between expression patterns and spatial correlations of P_{hetR}-*gfp* expression in ΔsepJ and ΔsepJΔfraCΔfraD filaments, we plotted scatterplots of the fluorescence intensities $f(n+1)$ of the $n+1$-th cell in a filament as a function of the fluorescence $f(n)$ of its nearest neighbor n along all filaments, as shown for the different strains in Figure 3. Under nitrogen-replete conditions, filaments of the three strains displayed a highly correlated behavior, with nearest-neighbor cells tending to exhibit similar fluorescence intensities, yielding significant positive correlations as measured by the Pearson correlation coefficients P (top panels, Figure 3). Note that the value of P for ΔsepJ filaments was somewhat smaller than for WT and ΔsepJΔfraCΔfraD filaments. Nitrogen deprivation brought about a large reduction in correlation in the three strains (middle panels, Figure 3), but particularly in the WT background, as a result of the large differences in fluorescence intensities between heterocysts and their nearest-neighbor vegetative cells. In contrast, the reduction in the ΔsepJ and ΔsepJΔfraCΔfraD backgrounds was smaller, due to the high expression from P_{hetR}-*gfp* in clusters of contiguous cells. Differences between patterns of expression in ΔsepJ and ΔsepJΔfraCΔfraD backgrounds were more evident if one considers the correlation between second neighbors along filaments ($f(n+2)$ as a function of $f(n)$, bottom panels in Figure 2B): whereas the Pearson correlation for the WT and ΔsepJ filaments was essentially zero, filaments of the ΔsepJΔfraCΔfraD background retained a non-negligible degree of correlation ($P = 0.24 \pm 0.04$). These results suggest that the lateral inhibition in the ΔsepJΔfraCΔfraD background was weaker than in the ΔsepJ background, resulting in more homogeneous cells. Furthermore, the results in this section suggest that under nitrogen deprivation, the effects of the ΔsepJ and ΔfraCΔfraD mutations may be non-additive and that the combined effect of deletion of sepJ and fraC-fraD partially preserves positive correlations such as those observed under nitrogen-replete conditions.

RNA-seq analysis

To understand better the effects of the deletions of the septal protein-encoding genes, we carried out RNA-seq experiments and compared the transcriptomes of the WT, ΔsepJ, and ΔsepJΔfraCΔfraD strains, both immediately (0 h) and 18 h after nitrogen stepdown. At this time, transcripts belonging to intermediate (6–12 h) and late (12–24 h) stages in the expression of genes from the network controlling heterocyst differentiation should be well represented (Flores et al., 2019). Although the fragmentation process giving rise to short filaments is known to commence right after nitrogen deprivation (Nürnberg et al., 2015), fragmentation was not complete 18 h after nitrogen stepdown, and filaments such as those shown in Figure 1 were observed. Analysis of four replicates for each condition was carried out to improve accuracy, after removal of ribosomal RNA (Transparent Methods). In total, 259.6 million sequence reads (up to 61 nt long) were mapped to the genome, and only reads with unique mapping, 54.5 million, were considered for further analysis. As an initial characterization and check of our experimental design, samples were
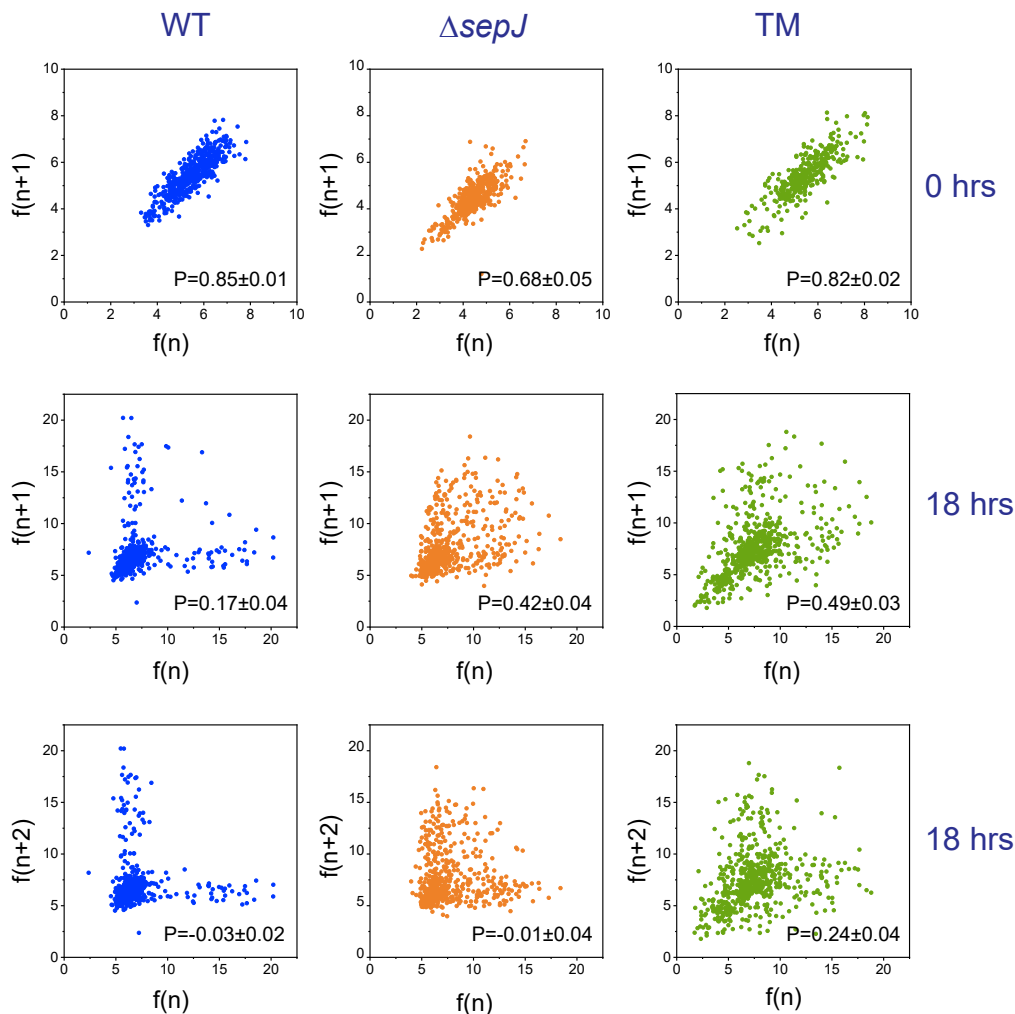
Figure 3. Correlated fluctuations along filaments

Scatterplots of the fluorescence intensity from P_{hetR}-*gfp* expression in cell pairs along filaments of WT, Δ*sepJ*, and Δ*sepJ*Δ*fraC*Δ*fraD* (TM) genetic backgrounds. Top row: scatterplots of the fluorescence intensity of the n+1-th cell in a filament, as function of the fluorescence intensity *f(n)* of the n-th cell, just after nitrogen deprivation (0 h). Middle row: *f(n+1)* versus *f(n)*, 18 h after nitrogen deprivation. Bottom row: *f(n+2)* versus *f(n)*, 18 h after nitrogen deprivation. Shown in all scatterplots are Pearson correlation coefficients P, with errors calculated from 10,000 bootstrap samples.

clustered using principal-component analysis (PCA). All genes with a sum count above 5 reads in all samples were used to carry out the PCA and predict the relatedness between samples. As shown in Figure S1, samples belonging to the different strains and grown under different conditions segregated into well-separated groups, and biological replicates clustered tightly together. No outlier values were detected, so all the replicates were used for further analyses. The first component PC1 explains 25.2% of the variance between samples and segregates these samples according to nitrogen availability. The second component PC2 explains 16.6% of the variance and shows a clear difference between the mutants and the WT strain, as well as between the mutant strains themselves (Figure S1).

Global analysis of changes resulting from acclimation to N depletion and deletion of septal protein genes

To identify unique patterns of transcriptional activity in the mutant strains relative to the WT, as well as between the different mutant strains themselves, we performed an unsupervised k-means clustering analysis of the data. As we detected a few cases of strong changes in expression of plasmid genes that could reflect genome rearrangements (e.g., deletions), we used the regularized log transformation values only for
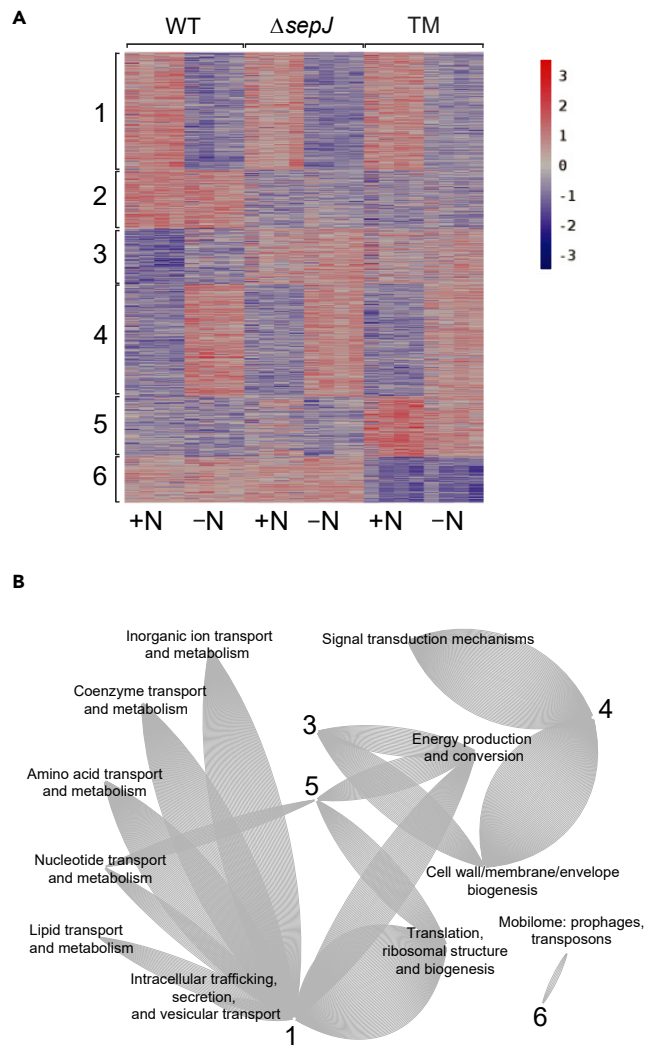
Figure 4. K-means clustering of differentially transcribed genes in WT, Δ*sepJ*, and Δ*sepJ*Δ*fraC*Δ*fraD* (TM) strains in the presence of nitrate (+N) and under nitrogen deprivation (-N)

(A) Normalized values of 3,712 chromosomal genes were used to run an unsupervised k-means analysis, setting k = 6. The legend shows the *z*-scores. The values were mean centered, and the colors scaled from −3 to 3 standard deviations.
(B) Network of differentially expressed genes and their association with enriched COG terms. Differentially expressed genes were clustered into six groups (using the K-means algorithm), based on their expression profile in the different strains (A). Enrichment analysis revealed 574 of these differentially expressed genes (represented by arcs) to be associated with enriched COG terms. Each gene is assigned to a gene expression cluster (numbers) based on its expression profile and is associated with an enriched COG term (labels). Note that in group 2 no COG terms were detected in this analysis. Enrichment analysis was performed using GProfiler (with a significant threshold of p < 0.05), and the network was constructed using CytoScape 3.7.2.

chromosomal genes that were differentially expressed (differential expression genes [DEG]). The RNA-seq data for the whole genome and for the DEG are found in Table S1. A k-means analysis was carried out both for nitrogen-replete and -poor conditions, taking into account the four biological replicates for each strain. To estimate a minimal value of clusters that show common expression profiles, we used the elbow method (Syakur et al., 2018). Although the method yields k = 4 as an optimal number of initial clusters (Figure S2), we found more informative to group the total of 3,712 genes into six clusters (k = 6), as shown in Figure 4A.

Cluster 1 includes genes that were expressed at high levels under nitrogen-replete conditions and were downregulated under nitrogen deprivation, whereas cluster 4 includes genes that exhibited the opposite

behavior, namely, genes that were expressed at low levels in nitrate-replete conditions and were upregulated under nitrogen deprivation (Figure 4A). Cluster 2 includes genes that in the WT were expressed independently of nitrogen availability and that were downregulated in both the ΔsepJ and ΔsepJΔfraCΔfraD mutants. Cluster 3 includes genes that in general were less expressed in the WT independently of nitrogen availability and were upregulated in both mutants. We attribute the effects of gene expression of clusters 2 and 3 to the ΔsepJ deletion, which is common to both mutants. Cluster 5 includes genes that were upregulated only in the ΔsepJΔfraCΔfraD mutant, independently of the nitrogen state, whereas cluster 6 represents the opposite behavior, namely, it includes genes that were downregulated only in the ΔsepJΔfraCΔfraD mutant. These last two clusters yield information about the effects of deletion of fraC and fraD. Most of the genes belonging to clusters 1 and 4 have been well studied during the last decades (Herrero et al., 2016; Flores et al., 2019). A glance at the data (Table S1, DEG_with_clusters sheet, filtering by cluster number) reveals that cluster 1 includes genes whose products are part of Photosystem II (e.g., psbV, psbC), Photosystem I (e.g., psaX, psaA, psaB), and phycobilisomes (e.g., pecA, pecB, pecC), as well as genes related to nitrate assimilation (e.g., nrtD, nrtC, nrtA, nirA, narB). In contrast, cluster 4 includes genes related to heterocyst differentiation (e.g., hesA, hetC, hepB, devA, patS, hetR) and other regulatory genes (e.g., patB, pknC, sigA).

The response to sepJ or fraC-fraD deletion of genes belonging to clusters 2, 3, 5, and 6 was previously unknown. To shed light on the behavior of these genes, we tested whether a category included in the Cluster of Orthologous Groups (COG) annotation was overrepresented in these clusters (Tatusov et al., 2000). For some of these genes, specifically for 574 differentially expressed genes, we obtained positive results that were used to construct a network that relates the different clusters with enriched COG categories (Figure 4B). Cluster 1 was enriched in five categories, related primarily with the transport and metabolism of amino acids, lipids, nucleotides, inorganic ions, and coenzymes, which exhibited higher expression under nitrate conditions. Cluster 4 showed enrichment in the Cell wall/membrane/envelope biogenesis and Signal transduction mechanisms categories. Genes in cluster 3 related to changes in Cell wall and Energy production categories were independent of nitrogen availability, whereas the genes in cluster 5 seem to be at an intermediate situation between clusters 3 and 1, as they belong to categories common to both clusters. We did not observe any enrichment in the case of genes belonging to group 2, and therefore this cluster is not represented in the network of Figure 4B. Enrichment in only one category (Mobilome) was observed in the case of cluster 6.

We additionally performed a gene ontology (GO) enrichment analysis using Ontologizer (Bauer et al., 2008) (Transparent Methods) and found in all clusters 2,999 enriched GO terms (see results in Table S2). Of these, 916 terms are found in cluster 5 and 401 terms in cluster 6, which gives further insight on the effects of the fraC-fraD deletions on the transcriptional landscape (clusters 5 and 6; Figure 4A). The results of this enrichment analysis for clusters 5 (upregulated genes) and 6 (downregulated genes) in the ΔsepJΔfraCΔfraD mutant compared with the ΔsepJ mutant show that upregulated genes included genes related to general cellular processes such as photosynthesis, development, and some amino acid and nucleotide biosynthesis pathways (for p value < 0.05, Table S2). Consistent with detection of photosynthesis-related genes, some encoded gene products were related to metal and cofactor binding as well as to electron transport. In contrast to upregulated genes, downregulated genes were related to a lower number of specific processes including nucleoside metabolism.

Identifying specific changes in transcription

To obtain a more refined picture of the transcriptional landscape and to identify pathways that are enriched in gene groups more than would be expected by chance, we performed a functional enrichment analysis of our RNA-seq data. DEG from comparisons between the ΔsepJ or ΔsepJΔfraCΔfraD mutants and the WT strain under both nitrogen-replete and -poor conditions were used for this enrichment analysis. Significantly enriched pathways are shown in Figure S3, based on either the COG (Tatusov et al., 2000) or the CyanoBase (Nakao et al., 2010) annotations.

Globally, when we compared both mutants against the WT strain under nitrate conditions, we observed some effects common to both mutants. Thus, both mutants exhibited upregulation of genes belonging to the Inorganic Ion Transporters category (Figure 5). Among those genes, transporter genes related to bicarbonate (HCO_3^-) uptake, which were among the most strongly affected, are considerably upregulated. These genes include those encoding the ABC transporter Cmp and the MFS low-affinity Na^+-bicarbonate
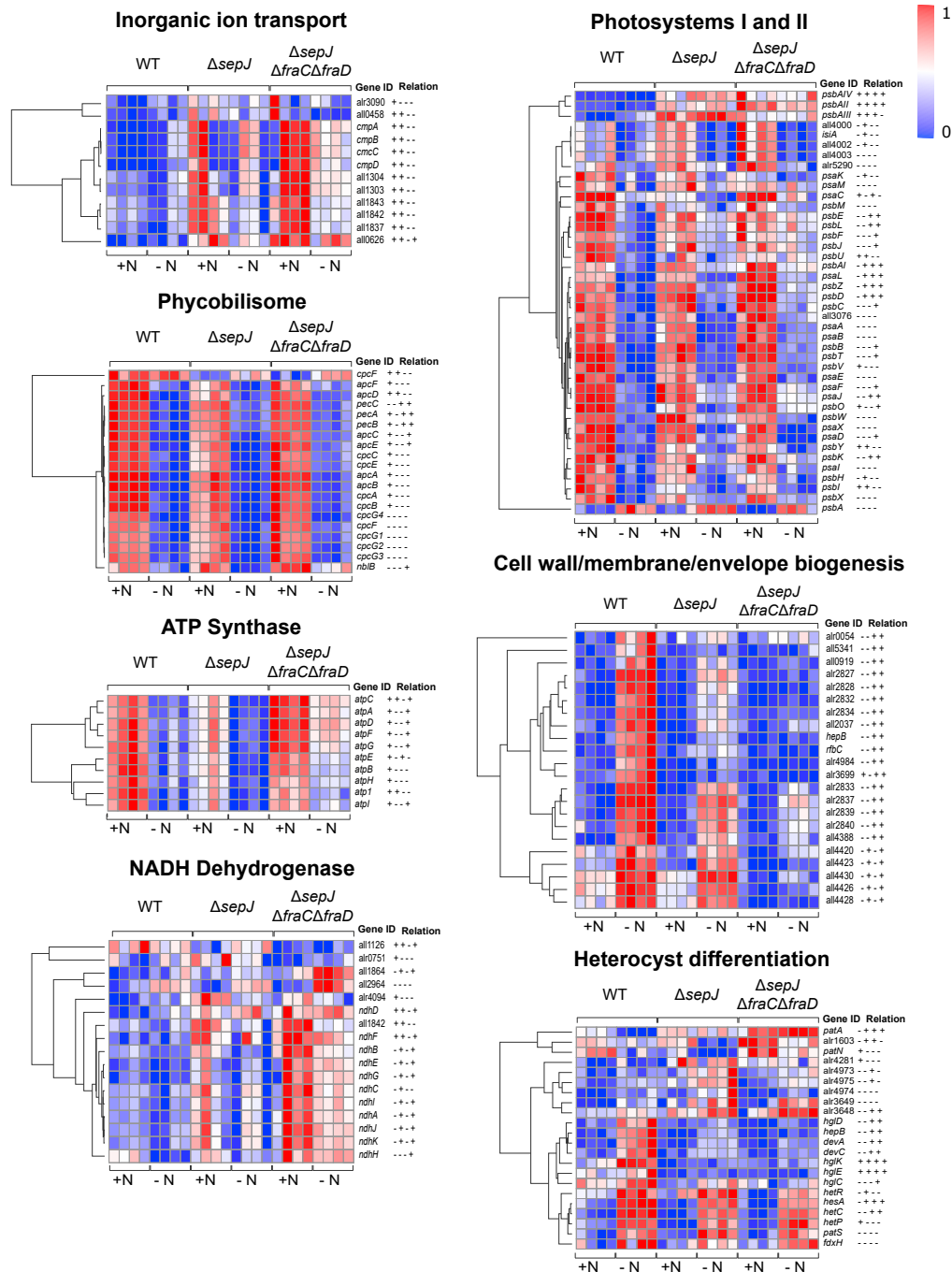
Figure 5. Hierarchical clustering heatmaps showing relative expression level of DEG in some selected enriched categories

Regularized-logarithm transformation expression values of DEG in each of four replicates for every strain and condition were used as input values. The color scale shows the differences between minimum (blue = 0) and maximum (red = 1) values in each row independently. Symbols + and − indicate whether there are significant differences in the comparison of the mutants with the wild-type strain or not, in this order: Δ*sepJ* versus WT (nitrate), Δ*sepJ*Δ*fraCD* versus WT (nitrate), Δ*sepJ* versus WT (no-nitrate), and Δ*sepJ*Δ*fraC*Δ*fraD* versus WT (no nitrate). Heatmaps of additional genes pertaining to the *Inorganic ion transport* and *Cell wall/membrane/envelope biogenesis* categories are shown in Figure S4.

co-transporter BicA (All1304) as well as its neighbor All1303, a putative Na^+/H^+ antiporter that may support BicA activity (the expression changes of these genes can be consulted in Table S3). The MFS high-affinity Na^+-bicarbonate co-transporter, SbtA (All2134), was also upregulated in response to *sepJ* inactivation (Table S3). Genes in the *all1843-all1837* cluster, which encode another putative Na^+/H^+ antiporter, were also highly upregulated (Figure 5). Finally, *all0626*, also highly upregulated, is a predicted Ca^{2+}/H^+ antiporter. All the components of the three known HCO_3^- transporters in *Anabaena* were upregulated with a fold change in the range 4–81 ($\log_2$FC of 2.13–6.35). We note that in addition to changes in the expression of carbon transporters (Figure 5), some changes in a wide repertory of transporters of other inorganic ions also took place (Figure S4).

Under nitrate conditions we observed, on the other hand, some differences between the mutant strains in categories related to *Energy Production*. For example, whereas the Δ*sepJ* mutant exhibited downregulation of phycobilisome and ATP synthase genes, the Δ*sepJ*Δ*fraC*Δ*fraD* mutant did not show this behavior (except for *cpcF*), and instead exhibited upregulation of some genes of the *Photosystem II* category and *NADH dehydrogenase* (NDH-1 or photosynthetic complex I, Schuller et al., 2020) (Figure 5). Within the *Photosystem II* category, expression changes were found for *psbAII, psbAIII,* and *psbAIV* genes that code for D1:2 isoforms of the D1 protein, which plays a key role in the PSII reaction center. The replacement of the native D1:1 isoform takes place under different stresses, such as under UV radiation (Sicora et al., 2006). Other genes such as *all4000, all4001,* (*isiA*) and *all4002*, whose products are homologous to the CP43 protein, and which play an essential role in the transmission of light energy to the photosynthetic reaction centers, also appeared in this category. (Note that *isiA* was placed by the automatic annotation as related to *Photosystem II*, although it is normally associated with *Photosystem I*). A very significant difference between the triple mutant and the Δ*sepJ* mutant under nitrate conditions was a 2.4- to 7.2-fold upregulation (2.3- to 4.2-fold upregulation in -N) of genes in the *alr1576-alr1586* cluster (see Table S1). Some of these genes encode extracytoplasmic proteins related to polysaccharide and sugar metabolism, including glycoside hydrolases, oxidases, and two proteins similar to xylose isomerase (xylose is found in the envelopes of heterocyst-forming cyanobacteria, Cardemil and Wolk, 1979).

Under nitrogen deprivation, the most statistically significant effect that was detected in the mutants was a strong downregulation of structural genes related to the *Cell wall/membrane/envelope biogenesis* category. Although this effect was present in both mutants, the repression of genes in this category was stronger in the Δ*sepJ*Δ*fraC*Δ*fraD* mutant (Figure 5). Among these structural genes, we found many related to the synthesis of the extra-cell envelope that surrounds heterocysts, which is composed of the heterocyst-specific polysaccharide (Hep) and heterocyst-specific glycolipid (Hgl) layers (Flores et al., 2019). Most of the *hep* genes located in the cluster *alr2823-alr2841*, also known as "HEP island," were downregulated in this category (Huang et al., 2005), as well as other genes such as *alr3698* (*hepB*) and *alr3699*, located outside of this region and also required for the formation of this layer (Wang et al., 2007). Some genes related to the synthesis of the Hgl layer (*hgl* genes) were also downregulated and were found in the *Heterocyst differentiation* category (Figures S3B and 5), as it was also the case for *devC* and *devA* genes that are involved in the deposition of this layer (Black et al., 1995; Fiedler et al., 1998) and *hglK* that is involved in septal maturation (Black et al., 1995; Arévalo and Flores, 2020). Among the structural genes that were downregulated, the gene cluster (*all4420-all4430*) is quite interesting because it showed this behavior in the Δ*sepJ*Δ*fraC*Δ*fraD* mutant but hardly in the Δ*sepJ* mutant (Figure 5). Some of the genes of this cluster encode glycosyl transferases or extracellular polysaccharide biosynthesis/transport proteins. We report on other genes within this category that displayed changes in their expression in Figure S4.

Finally, some metabolic effects previously detected in the nitrate-grown mutants remained stable after nitrogen deprivation (see Figure S3B, *Energy Production and Conversion*, in both mutants, and *ATP synthase, Photosystem II,* and *NADH dehydrogenase* in the Δ*sepJ*Δ*fraC*Δ*fraD* mutant). In addition, new upregulated gene categories related with protein synthesis, fatty acid metabolism, and CO_2 fixation arose in the Δ*sepJ*Δ*fraC*Δ*fraD* mutant under nitrogen deprivation. This last category includes the *rbcS* and *rbcL* genes that code for the small and large subunits of the CO_2-fixing enzyme Rubisco, the *ccmM* and *ccmN* genes that are related to carboxysomes (Turmo et al., 2017), and the *prk* gene that codes for phosphoribulokinase, a key enzyme in the Calvin-Benson-Bassham cycle and an important point of regulation for CO_2 fixation. In contrast, phycobilisome genes that under nitrate conditions were downregulated in the Δ*sepJ* mutant, appeared upregulated under nitrogen deprivation (Table S3).

Changes in expression of HetR-dependent genes

Given the importance of the HetR regulator in the heterocyst differentiation process, we checked whether the expression of HetR-regulated genes is altered in the septal protein mutants. For this purpose, we selected from our data genes that are known to be expressed under nitrogen deprivation in a HetR-dependent way (Brenes-Álvarez et al., 2019). In this work, genes were classified as early or late, depending on the specific time during heterocyst differentiation in which they displayed maximal expression. Most of these genes were well represented in our transcriptome and appeared upregulated under nitrogen deprivation in the WT strain. Septal mutants displayed changes in the expression of both early and late genes. Although we did not detect significant changes in *hetR* nor *patS* expression, both the Δ*sepJ*Δ*fraC*Δ*fraD* and the Δ*sepJ* mutants displayed downregulation of *ntcA* in a combined nitrogen-independent way (Figure 6). Interestingly, under nitrogen deprivation the Δ*sepJ*Δ*fraC*Δ*fraD* mutant displayed downregulation of *patX*, a widely distributed gene in cyanobacteria that appears to have a role very similar to that of *patS* during heterocyst differentiation in *Anabaena* (Figure 6) (Elhai and Khudyakov, 2018). Finally, upregulation of *patA* under nitrogen deprivation was observed in both mutants (Figure 5). PatA regulates the levels or activity of HetR (Risser and Callahan, 2008) and was recently shown to interact with SepJ and with some elements of the divisome (Valladares et al., 2020).

Validation of RNA-seq results by real-time quantitative polymerase chain reaction

To provide independent evidence for the validity of the gene expression results identified in the RNA-seq analysis, we carried out real-time quantitative polymerase chain reaction (RT-qPCR) measurements of two of the most differentially expressed genes in our analysis: *cmpB*, which is one of the most upregulated genes in both the Δ*sepJ* mutant and the Δ*sepJ*Δ*fraC*Δ*fraD* mutant independently of the nitrogen source, and *hepC*, which conversely, is one of the most downregulated genes. *cmpB* codes for a permease component of the bicarbonate (HCO_3^-) uptake Cmp complex (López-Igual et al., 2012), whereas the product of *hepC* resembles an UDP-galactose lipid carrier transferase (Huang et al., 2005). The expression profiles of these genes displayed the same tendency as that detected by RNA-seq, with only minor quantitative differences between the two methods (Figure 7).

Discussion

Heterocyst-forming cyanobacteria, organisms of ancient origin, represent one of the first successful attempts at creating a multicellular unit of selection in the history of life on Earth (Schirrmeister et al., 2013). Multicellularity and division of labor strongly hinge on cell-cell communication (Herrero et al., 2016). It is therefore of interest to test the extent to which disruption of intercellular communication affects the biology of the organism. In the present work, we studied the effects of altering the molecular transfer of nutrients and signals between cells by deleting selected septal proteins in *Anabaena* filaments, a model system of heterocyst-forming (multicellular) cyanobacteria in which the number of neighbors of each cell is well defined.

Although some differences in sugar transport, septal structure, and fragmentation between the WT, Δ*sepJ*, and Δ*sepJ*Δ*fraC*Δ*fraD* genetic backgrounds have been already described (Nürnberg et al., 2015), our experiments shed light on additional aspects in which these strains differ. In terms of growth, the two mutant strains grow similarly under nitrogen-replete conditions, but at a lower rate than the WT. On the other hand, cellular autofluorescence levels and absorbance of pigments of Δ*sepJ* filaments are lower than those of the WT, whereas those of Δ*sepJ*Δ*fraC*Δ*fraD* are higher, irrespective of whether these levels are measured before or 18 h after nitrogen deprivation. We note that some phycobilisome genes are downregulated already in the presence of nitrate in the *sepJ* mutant. The differences in autofluorescence as well as absorbance spectra between the three genetic backgrounds may also reflect different degrees of degradation of phycobilisomes, e.g., by NblA-dependent degradation (Baier et al., 2004), especially between the two mutant backgrounds (i.e., decreased phycobilisome degradation in the triple mutant when compared with the *sepJ* mutant). Phycobilisomes play a role in the antenna complex for photosynthesis and as a source of stored nitrogen (Bienert et al., 2006), and our RNA-seq results show that many genes within the *Phycobilisome* category were downregulated under nitrogen deprivation and the expression of some genes was altered in one or the two mutants analyzed (Figure 5).

The characterization of spatial patterns of expression of GFP from the promoter of the *hetR* gene, which encodes the master regulator of cell differentiation in *Anabaena*, also sharpens the differences between
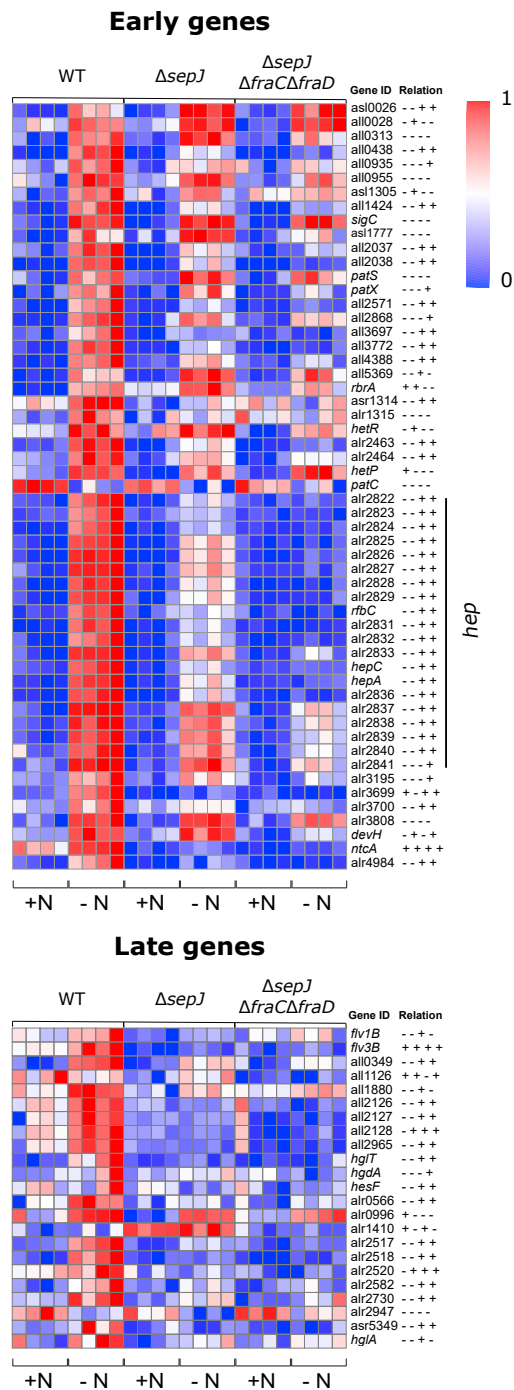
Figure 6. Heatmaps showing relative expression level of DEG related with heterocyst differentiation process, in the early and late stages of the process

DEG whose expression is induced under nitrogen deprivation and in a HetR-dependent way (Brenes-Álvarez et al., 2019) are showed in this analysis. Regularized-logarithm transformation expression values of these genes in each of four replicates for every strain and condition were used as input values. The color scale shows the differences between minimum (blue = 0) and maximum (red = 1) values in each row independently. Symbols + and − indicate whether there are significant differences in the comparison of the mutants with the WT strain or not, in this order: Δ*sepJ* versus WT (nitrate), Δ*sepJ*Δ*fraC*Δ*fraD* versus WT (nitrate), Δ*sepJ* versus WT (no nitrate), and Δ*sepJ*Δ*fraC*Δ*fraD* versus WT (no nitrate).
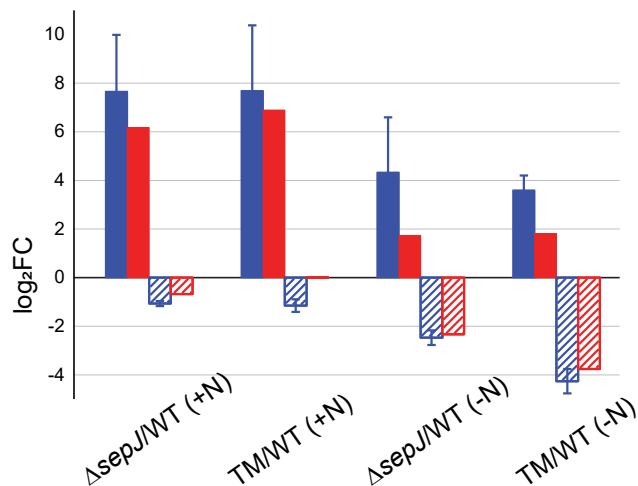
Figure 7. Validation of differentially expressed genes by real-time PCR

Comparison of RNA-seq (red) and RT-PCR (blue) measures of changes in expression of *cmpB* (positive changes) and *hepC* (negative changes) genes in the Δ*sepJ* mutant and the Δ*sepJ*Δ*fraC*Δ*fraD* (TM) mutant against the wild-type strain in the presence of nitrate and after nitrogen deprivation. All data are shown as means ± standard error (n = 3).

the behaviors of Δ*sepJ* and Δ*sepJ*Δ*fraC*Δ*fraD* filaments. Nearest-neighbor Pearson correlations are high in WT, Δ*sepJ*, and Δ*sepJ*Δ*fraC*Δ*fraD* filaments under nitrogen-replete conditions, whereas the weaker correlation between nearest-neighbor cells in Δ*sepJ* filaments relative to WT filaments is consistent with impaired transfer of a PatS-derived signal, as observed previously (Corrales-Guerrero et al., 2015; Mariscal et al., 2016). In contrast, under nitrogen-poor conditions, heterocysts are formed only in WT filaments, giving rise to off-diagonal contributions to the scatterplot of expression due to lateral inhibition and increased promoter activity of *hetR*. This results in a significant drop in correlation in WT filaments when compared with those of Δ*sepJ* and Δ*sepJ*Δ*fraC*Δ*fraD* backgrounds. Correlations between second neighboring cells capture better the difference between expression patterns in Δ*sepJ* and Δ*sepJ*Δ*fraC*Δ*fraD* filaments: whereas the Pearson coefficient is essentially zero for Δ*sepJ* filaments, correlations in Δ*sepJ*Δ*fraC*Δ*fraD* filaments are still significant. Note that in contrast to nearest-neighbor pairs, which include sister cells resulting from cell division, correlations between second neighboring cells are much weaker. One may hypothesize that the smoother, graded expression patterns observed in Δ*sepJ*Δ*fraC*Δ*fraD* filaments are consistent with a compensation in intercellular molecular transfer in the Δ*sepJ*Δ*fraC*Δ*fraD* compared with Δ*sepJ* background filaments. Such compensation might result from the absence of a FraD-containing plug that gates some septal junctions (Weiss et al., 2019).

The differences between filaments of the three genetic backgrounds in spatial patterns of expression and absorption spectra were more marked at late stages following nitrogen deprivation, in which the expression of genes controlling heterocyst differentiation should have taken place. This motivated an exploration of the transcriptome landscapes under both nitrogen-replete and -poor conditions. The transcriptomes revealed that deletion of septal proteins causes effects in the expression of several sets of genes, likely as a result of impaired cell-cell communication. A striking effect of *sepJ* inactivation and, further, of the combined inactivation of *sepJ*, *fraC*, and *fraD* is upregulation of bicarbonate uptake transporters including an ABC transporter and Na^+-bicarbonate co-transporters, accompanied by Na^+/H^+ antiporters that may be important to support the activity of the co-transporters. This may indicate a state of sensing C starvation in the mutants, resulting in induction of the transporters. The *all4444-all4445-all4446* operon encoding vegetative cell flavodiiron proteins is also upregulated in the Δ*sepJ* and Δ*sepJ*Δ*fraC*Δ*fraD* strains (Table S3), and this operon is known to be induced by CO_2 limitation (Allahverdiyeva et al., 2015; Picossi et al., 2015). These flavodiiron proteins are involved in the photo-protection of Photosystem II, which along with the NDH-1 complex is also upregulated in the mutants. It is noteworthy that this effect is noticeable particularly under nitrogen-replete conditions. How inactivation of the septal proteins leads to these effects is unknown, but it may be related to the impairment in the intercellular transfer of sucrose that appears to occur in the mutants (Nürnberg et al., 2015), which may result in uneven distribution of photosynthate along the filament. Formation of septal junctions, which mediate

intercellular molecular exchange, is impaired in the *sepJ* and *fraC-fraD* deletion mutants (Flores et al., 2018).

There are genes whose expression in the septal protein mutants is different from the WT but similar in both mutants (clusters 2 and 3), and can therefore be ascribed to the effects of *sepJ* deletion common to both mutants, whereas there are genes whose expression is primarily affected by the *fraC-fraD* deletion (clusters 5 and 6). Most of the genes in these clusters have not been annotated, and their function is unknown. The most striking effect in the Δ*sepJ*Δ*fraC*Δ*fraD* strain when compared with the Δ*sepJ* strain is induction of the *alr1576-alr1586* gene cluster, in which some genes encode enzymes that may catalyze exopolysaccharide and sugar modifications.

In line with previous results, we observed significant remodeling of the WT transcriptome following nitrogen deprivation (Flaherty et al., 2011), and in particular changes in the transcription of heterocyst differentiation genes controlled by the master regulator HetR (Brenes-Álvarez et al., 2019). As shown in Figure 6, the changes in HetR-controlled genes classified as representing early and late differentiation stages are similar for the WT, and timing differences may be accounted for by the different conditions of our experiments. These genes also highlight the differences between the transcriptomes of the Δ*sepJ* and Δ*sepJ*Δ*fraC*Δ*fraD* mutant strains. Among these differences, we detected changes in early genes that could affect heterocyst differentiation patterns, such as lower expression of *patX* that codes for a polypeptide similar to PatS and that can assist in lateral inhibition during heterocyst pattern formation (Elhai and Khudyakov, 2018), and overexpression of *patA*, whose product affects the levels and activity of the HetR regulator (Risser and Callahan, 2008).

Our results showing downregulation of heterocyst differentiation genes (some of which are included in the *Cell wall/membrane/envelope biogenesis* category) in the Δ*sepJ* and Δ*sepJ*Δ*fraC*Δ*fraD* strains are consistent with the known block in heterocyst differentiation caused by inactivation of *sepJ* (Flores et al., 2007), which as expected is evident only under N deprivation. Importantly, heterocyst differentiation starts in the *sepJ* mutants, but it is blocked after a thin Hep layer is deposited (Flores et al., 2007; Nayar et al., 2007). However, not all the genes included in the *Cell wall/membrane/envelope biogenesis* category have been previously related to heterocyst differentiation. This is the case, to the best of our knowledge, for the *all4420-all4430* gene cluster that appears to be involved in the production of extracellular polysaccharides and is specifically downregulated by deletion of *fraC-fraD*. Filament integrity in *Anabaena* is dependent on both cell wall components, the peptidoglycan mesh and the outer membrane (Burnat et al., 2014), and filament fragmentation by inactivation of *sepJ* or *fraC-fraD* is dependent on the activity of cell wall amidases (Bornikoel et al., 2017). Thus, our results showing downregulation, mainly under nitrogen deprivation, of *Cell wall/membrane/envelope biogenesis* genes suggest that a decreased level of the encoded proteins may contribute to the fragmentation of filaments previously reported (Nürnberg et al., 2015). Again, downregulation may result from a decreased intercellular molecular transfer in the mutants, in this case related to an impaired transfer of regulators (Rivers et al., 2014; Corrales-Guerrero et al., 2015; Mariscal et al., 2016).

Taken together, our results show how deletion of *sepJ*, *fraC*, and *fraD* genes that code for proteins that have a role in the formation of septal junctions (Flores et al., 2018) can have a broader impact on gene expression in *Anabaena* than previously thought. In addition to the more obvious effects of disruption of exchange of metabolites and signals between heterocysts and vegetative cells in a developed filament (Nürnberg et al., 2015), perturbations to cell-cell communication also have clear effects under nitrogen-replete conditions in which cells are undifferentiated. This underscores the benefits of intercellular communication even when all the cells along a filament may be functionally equivalent. A pooled metabolism facilitated by cell-cell communication may correct imbalances that may arise in one cell in isolation. Septal proteins can affect gene expression in two ways. On one hand, they play an important structural role, forming part of a highly organized and regulated superstructure such as the septum. Deletion mutants have an altered septum structure, and this alteration can conceivably influence processes that take place on this structure, such as peptidoglycan synthesis (Nürnberg et al., 2015). On the other hand, these proteins are crucial in the transfer of metabolites and signals between the cells that make up *Anabaena* filaments. Differences in the intercellular transfer of different molecular species (e.g., of regulators of heterocyst differentiation and nutrients such as sucrose) could account for most of the differences observed between the transcriptomes of these mutants, as well as between each mutant and the wild-type strain. Among these

differences, we observed changes in genes that belong to different categories, especially genes related to heterocyst differentiation, the cell wall, inorganic ion transport, carbon fixation, and photosynthesis. This underscores the fundamental function of septal junctions in a multicellular cyanobacterium such as *Anabaena*, going far beyond a role in the heterocyst differentiation process, participating in other processes such as the coordination of photosynthetic metabolism between the cells that are part of the same filament.

Limitations of the study

Deletion of septal proteins can have profound effects on a cyanobacterial organism of filamentary structure such as *Anabaena*. The present study sheds light on these effects, both under nitrogen-rich and -poor conditions, by investigating a *sepJ* deletion mutant and a *sepJ/fraC/fraD* triple deletion mutant. We found both global and specific effects in different mutants and nitrogen availability conditions. The transcriptome landscape mapping yields a comprehensive, broad analysis of these effects, whereas the resulting datasets invite further investigation to elucidate in-depth, specific effects of intercellular junction integrity on gene expression. Detailed studies to annotate and elucidate the function of genes, particularly those differentially affected in the triple mutant compared with the *sepJ* mutant, are called for to pinpoint at higher resolution the differences between the two mutants and the non-additivity of the *sepJ* and *fraC/fraD* deletions. For nitrogen deprivation our study was limited to 18 h after nitrogen stepdown. It will be interesting to explore the transcriptome landscape later, when mutant filaments are fully fragmented. Detailed studies of the transcriptomes at other times after nitrogen deprivation may also unravel other differences between the growth and survival of the *sepJ* and triple mutants that are not obvious at 18 h. Last, the effects of septal protein deletions on plasmid genes have not been analyzed due to possible genomic rearrangements. Future studies could address this aspect of gene expression and explore further the unique resources we are sharing with the community.

Resource availability

Lead contact

Further information and requests for resources and reagents should be directed to the Lead Contact, Joel Stavans (joel.stavans@weizmann.ac.il).

Materials availability

Strain CSVM12 will be made available upon request.

Data and code availability

The RNA-seq data generated in this study have been deposited in NCBI's Gene Expression Omnibus and are accessible through GEO Series accession number GSE161085 (https://www.ncbi.nlm.nih.gov/geo/query/acc.cgi?acc=GSE161085). The published article includes all the bioinformatics analysis reported in this study.

Methods

All methods can be found in the accompanying Transparent Methods supplemental file.

Supplemental information

Supplemental Information can be found online at https://doi.org/10.1016/j.isci.2020.101977.

Authors contribution

Conceptualization R.A.-G., E.F., and J.S.; Methodology V.M., R.A.-G., and J.S.; Validation D.L., B.D., R.A.-G., S.C., and J.S.; Formal Analysis D.L., B.D., S.C., R.A.-G., E.F., and J.S.; Investigation R.A.G. and S.C.; Resources V.M., D.L., B.D., E.F., S.C., R.A.-G., and J.S.; Data Curation D.L., B.D., R.A.-G., and J.S.; Writing –

Declaration of interests

The authors declare no competing interests.

References

Allahverdiyeva, Y., Isojärvi, J., Zhang, P., and Aro, E.-M. (2015). Cyanobacterial oxygenic photosynthesis is protected by flavodiiron proteins. Life *5*, 716–743.

Arévalo, S., and Flores, E. (2020). Pentapeptide-repeat, cytoplasmic-membrane protein HglK influences the septal junctions in the heterocystous cyanobacterium Anabaena. Mol. Microbiol. *113*, 794–806.

Baier, K., Lehmann, H., Stephan, D.P., and Lockau, W. (2004). NblA is essential for phycobilisome degradation in Anabaena sp. strain PCC 7120 but not for development of functional heterocysts. Microbiology *150*, 2739–2749.

Bauer, S., Grossmann, S., Vingron, M., and Robinson, P.N. (2008). Ontologizer 2.0 - a multifunctional tool for GO term enrichment analysis and data exploration. Bioinformatics *24*, 1650–1651.

Bienert, R., Baier, K., Volkmer, R., Lockau, W., and Heinemann, U. (2006). Crystal structure of NblA from Anabaena sp. PCC 7120, a small protein playing a key role in phycobilisome degradation. J. Biol. Chem. *281*, 5216–5223.

Black, K., Buikema, W.J., and Haselkorn, R. (1995). The hglK gene is required for localization of heterocyst-specific glycolipids in the cyanobacterium Anabaena sp. strain PCC 7120. J. Bacteriol. *177*, 6440–6448.

Bornikoel, J., Carrión, A., Fan, Q., Flores, E., Forchhammer, K., Mariscal, V., Mullineaux, C.W., Perez, R., Silber, N., Wolk, C.P., and Maldener, I. (2017). Role of two cell wall amidases in septal junction and nanopore formation in the multicellular cyanobacterium Anabaena sp. PCC 7120. Front. Cell. Infect. Microbiol. *7*, 1–15.

Brenes-Álvarez, M., Mitschke, J., Olmedo-Verd, E., Georg, J., Hess, W.R., Vioque, A., and Muro-Pastor, A.M. (2019). Elements of the heterocyst-specific transcriptome unravelled by co-expression analysis in *Nostoc* sp. PCC 7120. Environ. Microbiol. *21*, 2544–2558.

Burnat, M., Schleiff, E., and Flores, E. (2014). Cell envelope components influencing filament length in the heterocyst-forming cyanobacterium Anabaena sp. strain PCC 7120. J. Bacteriol. *196*, 4026–4035.

Cardemil, L., and Wolk, C.P. (1979). The polysaccharides from heterocyst and spore

envelopes of a blue-green alga. Structure of the basic repeating unit. J. Biol. Chem. *254*, 736–741.

Corrales-Guerrero, L., Tal, A., Arbel-Goren, R., Mariscal, V., Flores, E., Herrero, A., and Stavans, J. (2015). Spatial fluctuations in expression of the heterocyst differentiation regulatory gene hetR in Anabaena filaments. PLoS Genet. *11*, e1005031.

Elhai, J., and Khudyakov, I. (2018). Ancient association of cyanobacterial multicellularity with the regulator HetR and an RGSGR pentapeptide-containing protein (PatX). Mol. Microbiol. *110*, 931–954.

Fiedler, G., Arnold, M., Hannus, S., and Maldener, I. (1998). The DevBCA exporter is essential for envelope formation in heterocysts of the cyanobacterium Anabaena sp. strain PCC 7120. Mol. Microbiol. *27*, 1193–1202.

Flaherty, B.L., Van Nieuwerburgh, F., Head, S.R., and Golden, J.W. (2011). Directional RNA deep sequencing sheds new light on the transcriptional response of Anabaena sp. strain PCC 7120 to combined-nitrogen deprivation. BMC Genomics *12*, 332.

Flores, E., Pernil, R., Muro-Pastor, A.M., Mariscal, V., Maldener, I., Lechno-Yossef, S., Fan, Q., Wolk, C.P., and Herrero, A. (2007). Septum-localized protein required for filament integrity and diazotrophy in the heterocyst-forming cyanobacterium Anabaena sp. strain PCC 7120. J. Bacteriol. *189*, 3884–3890.

Flores, E., Picossi, S., Valladares, A., and Herrero, A. (2019). Transcriptional regulation of development in heterocyst-forming cyanobacteria. Biochim. Biophys. Acta Gene Regul. Mech. *1862*, 673–684.

Flores, E., Nieves-Morión, M., and Mullineaux, C. (2018). Cyanobacterial septal junctions: properties and regulation. Life *9*, 1.

Herrero, A., and Flores, E. (2019). Genetic responses to carbon and nitrogen availability in Anabaena. Environ. Microbiol. *21*, 1–17.

Herrero, A., Stavans, J., and Flores, E. (2016). The multicellular nature of filamentous heterocyst-forming cyanobacteria. FEMS Microbiol. Rev. *40*, 831–854.

Huang, G., Fan, Q., Lechno-Yossef, S., Wojciuch, E., Wolk, C.P., Kaneko, T., and Tabata, S. (2005). Clustered genes required for the synthesis of

heterocyst envelope polysaccharide in Anabaena sp. strain PCC 7120. J. Bacteriol. *187*, 1114–1123.

López-Igual, R., Picossi, S., López-Garrido, J., Flores, E., and Herrero, A. (2012). N and C control of ABC-type bicarbonate transporter Cmp and its LysR-type transcriptional regulator CmpR in a heterocyst-forming cyanobacterium, Anabaena sp. Environ. Microbiol. *14*, 1035–1048.

Lyons, N.A., and Kolter, R. (2015). On the evolution of bacterial multicellularity. Curr. Opin. Microbiol. *24*, 21–28.

Mariscal, V., Herrero, A., Nenninger, A., Mullineaux, C.W., and Flores, E. (2011). Functional dissection of the three-domain SepJ protein joining the cells in cyanobacterial trichomes. Mol. Microbiol. *79*, 1077–1088.

Mariscal, V., Nürnberg, D.J., Herrero, A., Mullineaux, C.W., and Flores, E. (2016). Overexpression of SepJ alters septal morphology and heterocyst pattern regulated by diffusible signals in *Anabaena*. Mol. Microbiol. *101*, 968–981.

Mariscal, V., Herrero, A., and Flores, E. (2007). Continuous periplasm in a filamentous, heterocyst-forming cyanobacterium. Mol. Microbiol. *65*, 1139–1145.

Merino-Puerto, V., Mariscal, V., Mullineaux, C.W., Herrero, A., and Flores, E. (2010). Fra proteins influencing filament integrity, diazotrophy and localization of septal protein SepJ in the heterocyst-forming cyanobacterium *Anabaena* sp. Mol. Microbiol. *75*, 1159–1170.

Merino-Puerto, V., Schwarz, H., Maldener, I., Mariscal, V., Mullineaux, C.W., Herrero, A., and Flores, E. (2011). FraC/FraD-dependent intercellular molecular exchange in the filaments of a heterocyst-forming cyanobacterium, Anabaena sp. Mol. Microbiol. *82*, 87–98.

Mullineaux, C.W., Mariscal, V., Nenninger, A., Khanum, H., Herrero, A., Flores, E., and Adams, D.G. (2008). Mechanism of intercellular molecular exchange in heterocyst-forming cyanobacteria. EMBO J. *27*, 1299–1308.

Nakao, M., Okamoto, S., Kohara, M., Fujishiro, T., Fujisawa, T., Sato, S., Tabata, S., Kaneko, T., and Nakamura, Y. (2010). CyanoBase: the cyanobacteria genome database update 2010. Nucleic Acids Res. *38*, D379–D381.

Nayar, A.S., Yamaura, H., Rajagopalan, R., Risser, D.D., and Callahan, S.M. (2007). FraG is necessary for filament integrity and heterocyst maturation in the cyanobacterium Anabaena sp. strain PCC 7120. Microbiology 153, 601–607.

Nürnberg, D.J., Mariscal, V., Bornikoel, J., Nieves-Morión, M., Krauß, N., Herrero, A., Maldener, I., Flores, E., and Mullineaux, C.W. (2015). Intercellular diffusion of a fluorescent sucrose analog via the septal junctions in a filamentous cyanobacterium. mBio 6, e02109.

Di Patti, F., Lavacchi, L., Arbel-Goren, R., Schein-Lubomirsky, L., Fanelli, D., and Stavans, J. (2018). Robust stochastic Turing patterns in the development of a one-dimensional cyanobacterial organism. PLoS Biol. 16, e2004877.

Pernil, R., Picossi, S., Mariscal, V., Herrero, A., and Flores, E. (2008). ABC-type amino acid uptake transporters Bgt and N-II of Anabaena sp strain PCC 7120 share an ATPase subunit and are expressed in vegetative cells and heterocysts. Mol. Microbiol. 67, 1067–1080.

Picossi, S., Flores, E., and Herrero, A. (2015). The LysR-type transcription factor PacR is a global regulator of photosynthetic carbon assimilation in Anabaena. Environ. Microbiol. 17, 3341–3351.

Ramos-León, F., Arévalo, S., Mariscal, V., and Flores, E. (2018). Specific mutations in the permease domain of septal protein SepJ differentially affect functions related to

multicellularity in the filamentous cyanobacterium. Microb. Cell 5, 555–565.

Risser, D.D., and Callahan, S.M. (2008). HetF and PatA control levels of HetR in Anabaena sp. strain PCC 7120. J. Bacteriol. 190, 7645–7654.

Rivers, O.S., Videau, P., and Callahan, S.M. (2014). Mutation of sepJ reduces the intercellular signal range of a hetN-dependent paracrine signal, but not of a patS-dependent signal, in the filamentous cyanobacterium Anabaena sp. strain PCC 7120. Mol. Microbiol. 94, 1260–1271.

Schirrmeister, B.E., De Vos, J.M., Antonelli, A., and Bagheri, H.C. (2013). Evolution of multicellularity coincided with increased diversification of cyanobacteria and the Great Oxidation Event. Proc. Natl. Acad. Sci. U S A 110, 1791–1796.

Schuller, J., Saura, P., Thiemann, J., Schuller, S., Gamiz-Hernandez, A., Kurisu, G., Nowaczyk, M., and Kaila, V. (2020). Redox-coupled proton pumping drives carbon concentration in the photosynthetic complex I. Nat. Commun. 11, 1–7.

Sicora, C.I., Appleton, S.E., Brown, C.M., Chung, J., Chandler, J., Cockshutt, A.M., Vass, I., and Campbell, D.A. (2006). Cyanobacterial psbA families in Anabaena and Synechocystis encode trace, constitutive and UVB-induced D1 isoforms. Biochim. Biophys. Acta 1757, 47–56.

Syakur, M.A., Khotimah, B.K., Rochman, E.M.S., and Satoto, B.D. (2018). Integration K-means

clustering method and elbow method for identification of the best customer profile cluster. IOP Conf. Ser. Mater. Sci. Eng. 336, 012017.

Tatusov, R.L., Galperin, M.Y., Natale, D.A., and Koonin, E.V.((2000). The COG database: a tool for genome-scale analysis of protein functions and evolution. Nucleic Acids Res. 28, 33–36.

Turmo, A., Gonzalez-Esquer, C.R., and Kerfeld, C.A. (2017). Carboxysomes: metabolic modules for CO2 fixation. FEMS Microbiol. Lett. 364, 176.

Valladares, A., Velázquez-Suárez, C., and Herrero, A. (2020). Interactions of PatA with the divisome during heterocyst differentiation in Anabaena. mSphere 5, e00188–20.

Wang, Y., Lechno-Yossef, S., Gong, Y., Fan, Q., Wolk, C.P., and Xu, X. (2007). Predicted glycosyl transferase genes located outside the HEP island are required for formation of heterocyst envelope polysaccharide in Anabaena sp. strain PCC 7120. J. Bacteriol. 189, 5372–5378.

Weiss, G., Kieninger, A., Maldener, I., Forchhammer, K., and Pilhofer, M. (2019). Structure and function of a bacterial gap junction analog. Cell 178, 374–384.

Wilk, L., Strauss, M., Rudolf, M., Nicolaisen, K., Flores, E., Kühlbrandt, W., and Schleiff, E. (2011). Outer membrane continuity and septosome formation between vegetative cells in the filaments of Anabaena sp. PCC 7120. Cell. Microbiol. 13, 1744–1754.

Supplemental Information

Impaired cell-cell communication in the multicellular

cyanobacterium *Anabaena* affects carbon

uptake, photosynthesis, and the cell wall

Sergio Camargo, Dena Leshkowitz, Bareket Dassa, Vicente Mariscal, Enrique Flores, Joel Stavans, and Rinat Arbel-Goren

Supplemental Information
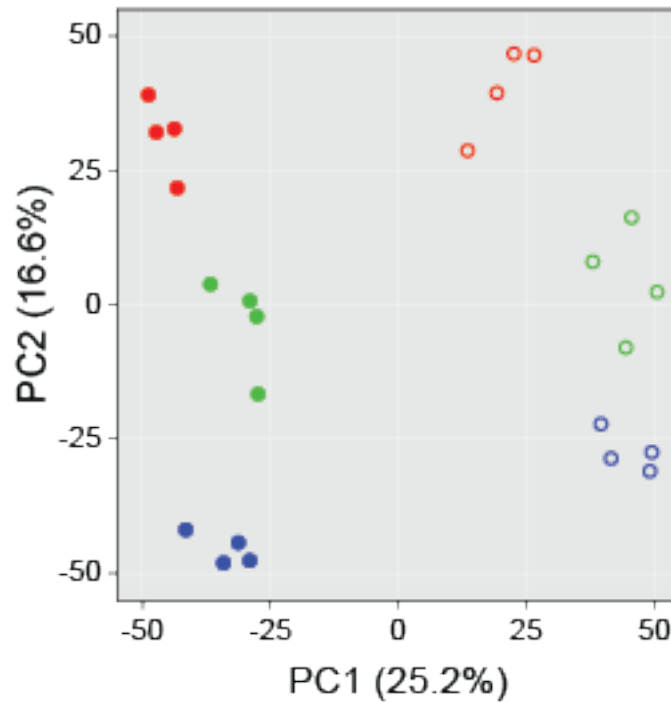
Supplemental data

Figure S1. Principal component analysis (PCA) of RNA-seq samples, Related to Figure 4A
The first principal component of variance PC1 as a function of the second PC2. Together, PC1 and PC2 comprise 41.8% of the variance in the data. Full circles denote samples grown under nitrogen-replete conditions (BG11 medium), whereas empty circles denote samples grown under nitrogen depleted conditions (BG11$_0$ medium). Colors represent different genetic backgrounds: wild-type (blue), ΔsepJ (green) and ΔsepJΔfraCΔfraD (red). Each four identical symbols represent four independent experimental replicates.
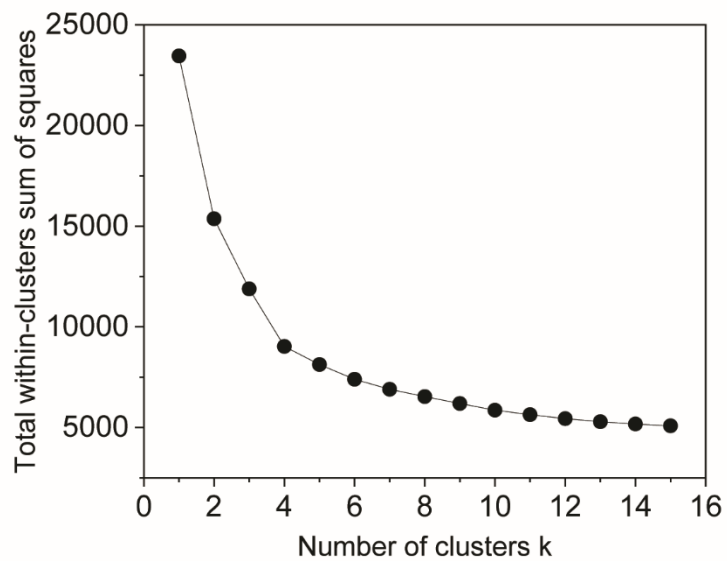
Figure S2.   Total sum of squares within each cluster and between clusters for the determination of optimal number of clusters in a k-means analysis, Related to Figure 4A. According to the elbow method, one should choose a k such that additional clusters do not substantially reduce sum of squares. This can lead to a k of 4. However, we found it helpful to use a k value that is slightly larger than this. k=6 was chosen.
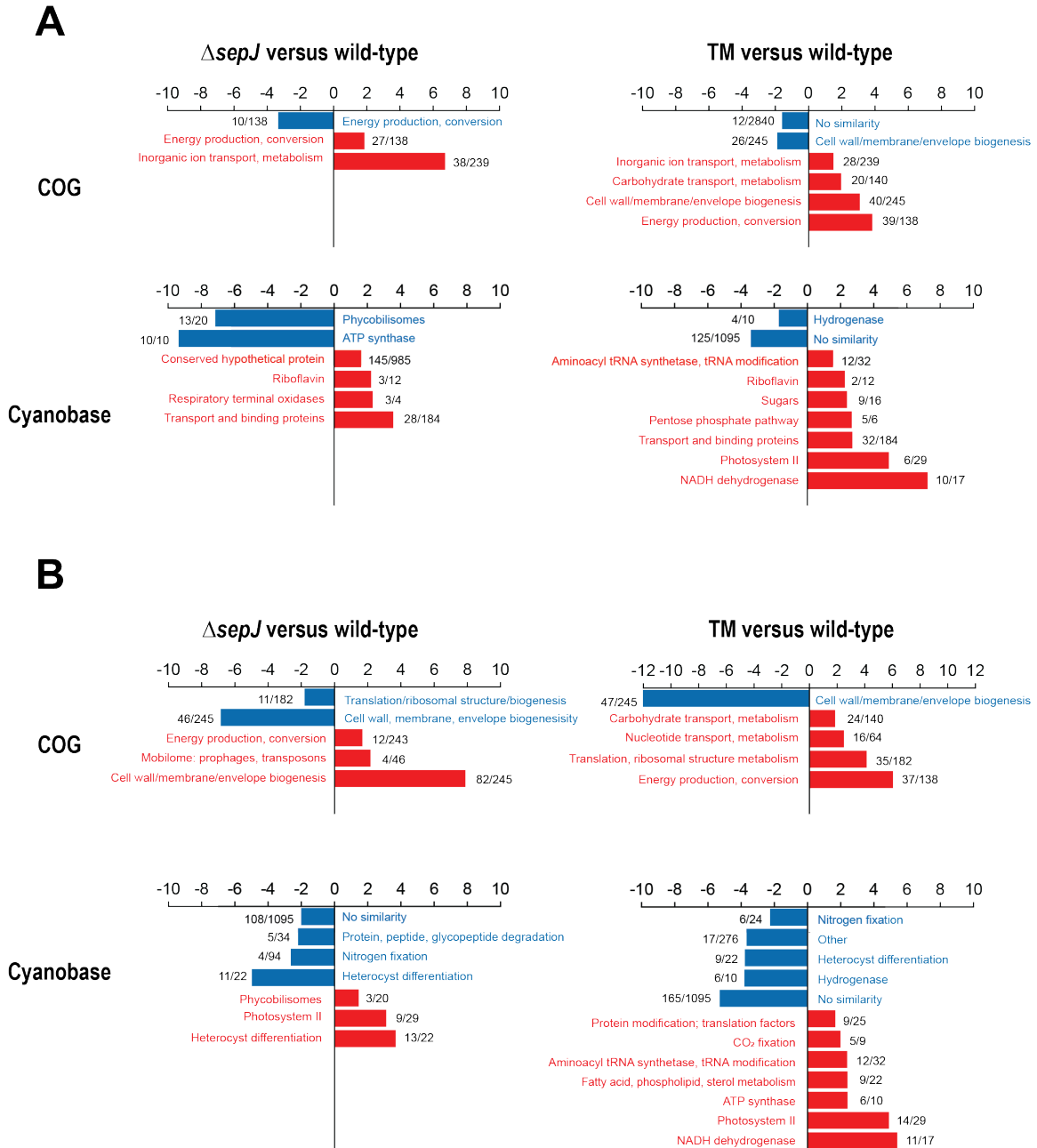
Figure S3. **Gene set enrichment analysis of ΔsepJ and ΔsepJΔfraCΔfraD (TM) mutants in comparison with wild-type _Anabaena_ (strain PCC 7120), Related to Figure 4A.** Strains grown in the presence of nitrate (A) or incubated under nitrogen deprivation (B) are compared. The degree of enrichment is represented by $\log_{10}$ of the p adjust value for multiple testing statistical analysis. Note that COG annotation (Tatusov _et al._, 2000) has broader categories than the Cyanobase annotation (Nakao _et al._, 2010), and that a category in the former may include many categories in the latter. The ratio adjacent to each bar represents the number genes that changed relative to the total number of genes in the indicated category.
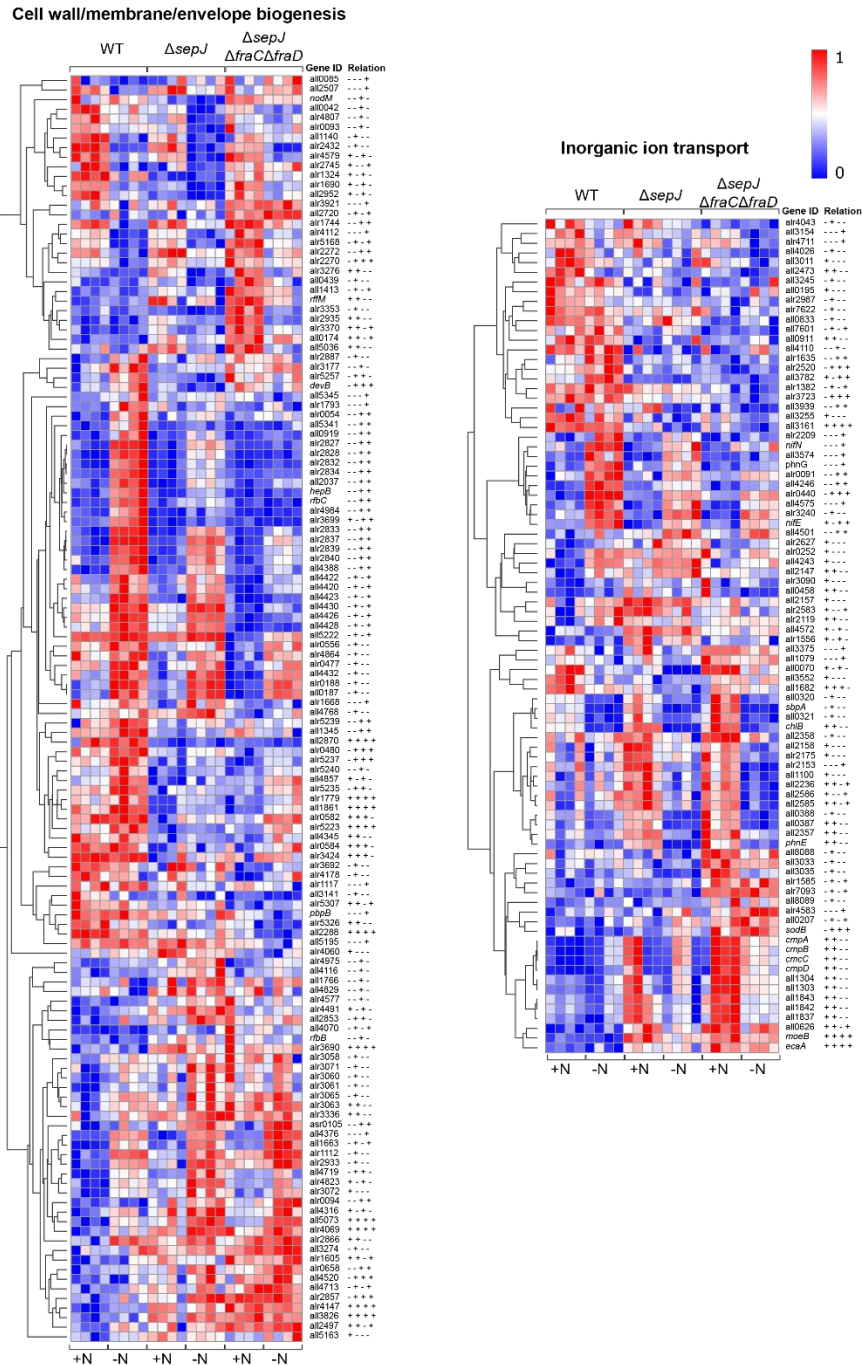
Figure S4. Hierarchical clustering heat maps of relative expression level of all DEG in selected categories detected in the gene set enrichment analysis (GSEA), Related to Figure 4A and Figure 5. Regularized-logarithm transformation expression values of genes in each of four replicates for every strain and condition were used as input values. All genes had a p-adjusted value (padj) <0.05. The color scale shows the differences between minimum (blue=0) and maximum (red=1) values in each row independently. Symbols + and - indicate whether there are significant differences in the comparison of the mutants with the WT strain or not, in this order: Δ*sepJ* vs WT (nitrate), Δ*sepJ*Δ*fraC*Δ*fraD* vs WT (nitrate), Δ*sepJ* vs WT (no nitrate) and Δ*sepJ*Δ*fraC*Δ*fraD* vs WT (no nitrate).

Transparent Methods

Bacterial strains and growth conditions. The *sepJ*, *fraC*, and *fraD* genes are open reading frames *alr2338*, *alr2392*, and *alr2393* of the *Anabaena* genome, respectively (Kaneko *et al.*, 2001). Strain CSVM34 is a deletion mutant of *sepJ* and strain CSVM141 a triple deletion mutant of *sepJ*, *fraC* and *fraD* genes that have been previously described (Mariscal *et al.*, 2011; Nürnberg *et al.*, 2015). Strain CSVM12 is a Δ*sepJ*Δ*fraC*Δ*fraD* mutant that bears a translational fusion of *hetR* with *gfp*-mut2 reporter integrated in its chromosome. This strain was constructed in the same way as CSL64 (WT background with *hetR-GFP*) and CSVM10 (Δ*sepJ* with *hetR-GFP*) strains, previously described (Corrales-Guerrero *et al.*, 2015).

Wild-type *Anabaena* (*Nostoc*) sp. strain PCC 7120 and derived mutant strains were grown photo-autotrophically in BG11 medium containing nitrate (Rippka *et al.*, 1979), or BG11$_0$ medium (lacking nitrate) at 30º C in the light (25 µE m$^{-2}\cdot$s^{-1} from led lamps) in shaken (180 rpm) liquid cultures or in medium solidified with 1% (w/v) Difco Agar. When required for strains CSL64, CSVM10 and CSVM12, antibiotics, streptomycin sulfate (Sm) and spectinomycin dihydrochloride pentahydrate (Sp), were added to the media, at final concentrations of 2 µg/mL for liquid and 5 µg/mL for solid media. For transfer between media, cells were harvested by centrifugation (3000 × *g*) and washed three times with the appropriate medium.

Filament growth. Time-lapse microscopy images of wild-type *Anabaena*, CSVM34 and CSVM141 derived mutant filaments growing in BG11 medium were used to calculate the doubling time of the three strains. The doubling time $t_d = ln2/\mu$, where μ is the growth rate, was calculated from the increase in the number of cells in a given filament as a function of time.

Whole cell spectra. Intact cells of wild-type *Anabaena* and CSVM34 and CSVM141 derived mutant strains were adjusted to OD$_{750}$=0.4 in liquid cultures containing nitrate or subjected to nitrogen deprivation and were grown for the number of hours indicated in each case under the standard conditions described before. Spectra of different cultures were taken between 350 and 750 nm on a Jasco V-630 spectrophotometer, as previously described (Ogawa *et al.*, 2013). To account for the effect of instrument noise and differences of light scattering due to possible small differences in growth rate between strains we perform a baseline subtraction of absorbance at 750 nm, taking for each sample the absorbance value at this wavelength, and subtracting this value for all the wavelengths of the respective spectrum.

Samples for time-lapse microscopy. For time-lapse, single cell measurements of *Anabaena*, 5µl of culture were pipetted onto an agarose low-melting gel pad (1.5%) in BG11$_0$ medium containing 10 mM NaHCO$_3$, which was placed on a microscope slide. The pad with the cells was then covered with a #0 mm coverslip and then placed on the microscope at 30°C and the cells grew with light from external LED and the intensity of illumination was ≈25-30 µE m^{-2}s^{-1}. Filament growth within these devices are similar to those in bulk cultures (Corrales-Guerrero *et al.*, 2015). Images were taken every 30 min on a Nikon Eclipse Ti-E microscope controlled by the NIS-Elements software using a 60 N.A 1.40 oil immersion phase contrast objective lens (Nikon plan-apochromat 60x NA=1.40) and an Andor iXon X3 EMCCD camera. Focus was maintained throughout the experiment using a Perfect Focus System (Nikon). All the filters used are from Chroma. The filters used were ET480/40X for excitation, T510 as dichroic mirror, ET535/30m for emission (GFP set) and ET430/24x for excitation, 505dcxt as dichroic mirror, and HQ6001p for emission (autofluorescence measurements). Samples were excited with a pE-2 fluorescence LED illumination system (CoolLED).

Image segmentation and processing. All image processing and data analysis were performed using MATLAB (MathWorks) as described previously (Di Patti *et al.*, 2018). Filament and individual cell recognition were performed on phase contrast images using an algorithm developed in our laboratory. The segmentation was checked in all experiments, and corrected manually for errors in recognition. Standard edge detection was used to find the filament outline and then locate the barrier

between the cells. A first order approximation to the center of each cell was first found, using a method that first identifies regions that are likely to be centers of cells; this is done by a series of morphological operations of dilation, closing and gradient on the phase contrast image. After this a point a center of each cell is identified (there may be false positives but this does not interfere with the algorithm). The centers were then arranged in the order they appear within the filament. For each center the closest center is found with a criterion that the line connecting the two points does not include values over a given cut-off. The criterion was used to prevent cases where the closest cell belongs to an adjacent filament; in such cases the line connecting the centers crosses the edge of the filament which has a high pixel value hence the cutoff. Next, the midpoint between two centers was calculated, to separate the cells along this line. For each midpoint the nearest points along the edge that are on opposite sides of the line connecting the centers of the cells were found. Finally a line was drawn between the two edge points that were identified as a pair across one another. After application of a threshold, the resulting labeled regions constitute the cells. Each segmented image was checked by hand. After all cells have been labeled, the data from the images is extracted; this includes the area, the mean fluorescence (GFP channel) and the mean autofluorescence for each cell in each frame. Finally the background fluorescence is measured in each image as an average of a background region of interest and subtracted from the measured mean GFP fluorescence. The wild-type background fluorescence was also measured but not subtracted in the analysis.

Preparation of RNA samples. For RNA sequencing (RNA-seq) and real time quantitative polymerase chain reaction (RT- qPCR) experiments, total RNA was prepared from strain PCC 7120, CSVM34 (ΔsepJ mutant) and CSM141 (ΔsepJΔfraCΔfraD mutant) in four biological replicates. Briefly, these strains were cultured in 100 ml of BG11 liquid medium in 250-ml flasks with cotton plugs until a concentration of 3-5 µg Chl · ml^{-1} was reached, then these cultures were collected, washed 3 times with $BG11_0$ medium and used to set 50 ml cultures (at 2 µg Chl · ml^{-1}) in nitrate conditions (BG11) and under nitrogen deprivation ($BG11_0$). Strains under these conditions were incubated for 18 hours under standard growth conditions. For each sample, cells were rapidly collected by filtration and washed with buffer TE_{50} (50 mM Tris-HCl [pH 8.0], 100 mM EDTA). Cells were resuspended in 2 ml of buffer TE_{50} and transferred to 2-ml tubes, and then they were collected by centrifugation at 11.500 x g for 2 minutes at 4°C. Supernatant was removed and cell pellets were flash frozen in nitrogen liquid for storage at -80°C. Total RNA was isolated by using hot phenol as described (Mohamed and Jansson, 1989) with modifications. All samples were treated with DNase I (Turbo DNA-free kit; Invitrogen). RNA quantity and purity were assessed with a Nanodrop One spectrophotometer and by agarose gel electrophoresis.

RT-qPCR measurements. For cDNA synthesis, 600 ng of total RNA of each sample was used for reverse transcription with the Quantitec Reverse Transcription kit (Qiagen). Then PCR amplification of 17.4 ng of each cDNA was carried out using Fast SYBR Green Master Mix (Applied Biosystems) that includes an internal reference based on the ROX™ dye, and the specific oligodeoxynucleotide primers (sequences 5' to 3'): all5167-1 (forward GCTCAAGCAATTCGTCACTGTTCC) and all5167-2 (reverse AAAGATTGCGTCGGTCTGGTGT); rnpB-1 (forward CTCTTGGTAAGGGTGCAAAGGTG) and rnpB-4 (reverse GGCTCTCTGATAGCGGAACTGG); alr2834-1 (forward GAATGTATTGCGGGGAGAAATG) and alr2834-4 (reverse GACGCAGGGTATTTTGAATGGAT); alr2878-1 (forward TCCTCATTCCTGCTGCCTTACC) and alr2878-4 (reverse CAAACCCACTGCACCAATGTAA). The amplification protocol was: one cycle at 95°C for 10 min; 40 cycles of: 95°C for 15 sec, and 60°C for 60 sec. RT-qPCR was carried out using an Applied Biosystems StepOnePlus instrument equipped with the StepOne Software v2.3. After the amplification was completed, a melting point calculation protocol was carried out in order to check that only the correct product was amplified in each reaction. The transcript levels of *hepC* (*alr2834*) and *cmpB* (alr2878) were normalized to the transcript levels of the housekeeping genes *rnpB* and *all5167* (*ispD*). Reactions were run in triplicate in three independent experiments.

Removal of ribosomal RNA for RNA-seq measurements. About 85% of prokaryotic total RNA corresponds to ribosomal RNA (rRNA), and therefore more than ~80% of the cDNA can hybridize with ribosomal regions, producing a bias in the subsequent analysis (Petrova *et al.*, 2017). To

minimize this effect and exclude Ribosomal RNA from the 700 ng of total RNA we used Ribozero rRNA removal kit Bacteria (Illumina) according to the manufacturer's instructions. We achieved an average reduction in rRNA of 67% per sample. The rest of ribosomal sequences was removed by bioinformatics methods prior to alignment of sequences against the reference genome.

Library preparation and sequencing. The cDNA libraries were prepared by Genomic core facilities (Weizmann Institute of Science, Israel) using their in-house protocol for RNA-seq. Briefly, reverse transcription was done with random hexamers on 70ng RNA followed by fragmentation and synthesis of double-stranded cDNA. Then, end repair, adenosine base addition, adapter ligation and PCR amplification steps were performed. Libraries were evaluated by Qubit (Thermo Fisher scientific) and TapeStation (Agilent). Sequencing libraries were constructed with barcodes to allow multiplexing of 24 samples in 1 lanes. About 9.3 to 13M single-end 60-bp reads were sequenced per sample on Illumina HiSeq 2500 V4 instrument.

Transcriptome analysis. Raw reads were quality trimmed using Cutadapt (Martin, 2013) (-q 20 -m 25) in addition to removal of sequencing adapters. In order to deplete rRNA genes *in silico*, reads were mapped to the 5S, 16S, 28S rRNA genes of strain PCC 7120 using Bowtie2 (Langmead and Salzberg, 2012) in end-to-end mode. Reads which did not map to rRNA genes were further used for the analysis of gene expression, and were aligned to the bacterial genome (GCA_000009705.1_ASM970v1) using Bowtie2 in end-to-end mode. Gene quantification was done using HTseq (in union mode) (Anders, Pyl and Huber, 2015). The final number of reads per sample are found in Table S1.

Normalization and analysis of differentially expressed genes was done using DESeq2 package version 1.22.2 (Love, Huber and Anders, 2014), and R version 3.5.0, using a model combining genotype and treatment into a single factor. A detailed study of differentially expressed genes in plasmids revealed that they had suffered rearrangements. For this reason, the genes of *Anabaena* plasmids were not included in the analysis. We also filtered out genes with a sum of less than 5 counts in all samples, resulting in 5941 genes. PCA was carried out using R and function prcomp using the normalized log values (rld). We compared each genotype to growth with and without nitrate, and each growth condition (nitrate) between the different genotypes. Differentially expressed genes were selected as genes with adjusted p value=<0.05 (Benjamini-Hochberg (Benjamini and Hochberg, 1995)) and minimal base mean of 5. No threshold of fold change was applied, in order to account for the heterogeneity of the different cell types. Clustering of gene expression values (rld) was applied using k-means method with 6 clusters using R (pheatmap and kmeans functions).

Functional annotation, gene ontology and enrichment analysis. Functional annotation of genes was inferred using COG (Tatusov *et al.*, 2000) and CyanoBase (Nakao *et al.*, 2010) databases. Different gene datasets were obtained from different comparisons between strains and growth conditions. A total of 3210 chromosomal differentially expressed genes were filtered out by the following two criteria log_2FC (fold change)≥ 0 and adjusted p value< 0.05. Then, filtered data were ordered from highest to lowest FC values; lowest to highest adjusted p value (upregulated genes); $log_2FC \leq 0$ and adjusted p value < 0.05, ordered from lowest to highest FC values and lowest to highest p value (downregulated genes). Annotation of genes from the aforementioned databases was used to construct a custom GMT file, which was used for pathways enrichment analysis with gProfiler (Raudvere *et al.*, 2019) (https://biit.cs.ut.ee/gprofiler/gost), with a significance cutoff of 0.05. Heatmaps of gene expression were constructed using standardized (z score) log2 transformed values (rld), in which the genes were hierarchically clustered using "one minus Pearson correlation" method and visualized using Morpheus (https://software.broadinstitute.org/morpheus/). Network of differentially expressed genes which were associated with enriched COG terms was constructed using CytoScape 3.7.2 (Shannon *et al.*, no date). Gene Ontology (GO) annotation was downloaded from UniprotKB knowledgebase for Nostoc sp. (strain PCC 7120). Enrichment analysis was done using Ontologizer (Bauer *et al.*, 2008) with Topology-Elim algorithm p<0.05) using differentially expressed genes in each cluster. As a background we used all annotated genes.

Supplemental References

Anders, S., Pyl, P. T. and Huber, W. (2015). HTSeq-A Python framework to work with high-throughput sequencing data, Bioinformatics, 31, 166–169.

Bauer, S. *et al.* (2008). Ontologizer 2.0 - A multifunctional tool for GO term enrichment analysis and data exploration, Bioinformatics, 24, 1650–1651.

Benjamini, Y. and Hochberg, Y. (1995). Controlling the False Discovery Rate: A Practical and Powerful Approach to Multiple Testing, J. R. Stat. Soc. Ser. B, 57, 289–300.

Corrales-Guerrero, L. *et al.* (2015). Spatial Fluctuations in Expression of the Heterocyst Differentiation Regulatory Gene hetR in Anabaena Filaments, PLoS Genet, 11, e1005031.

Kaneko, T. *et al.* (2001). Complete Genomic Sequence of the Filamentous Nitrogen-fixing Cyanobacterium Anabaena sp. Strain PCC 7120, DNA Res., 8, 205–213.

Langmead, B. and Salzberg, S. L. (2012). Fast gapped-read alignment with Bowtie 2, Nat. Methods, 9, 357–359.

Love, M. I., Huber, W. and Anders, S. (2014). Moderated estimation of fold change and dispersion for RNA-seq data with DESeq2., Genome Biol., 15, 550.

Mariscal, V. *et al.* (2011). Functional dissection of the three-domain SepJ protein joining the cells in cyanobacterial trichomes, Mol. Microbiol., 79, 1077–1088.

Martin, M. (2013). Cutadapt removes adapter sequences from high-throughput sequencing reads, EMBnet.journal, 17, 10–12.

Mohamed, A. and Jansson, C. (1989). Influence of light on accumulation of photosynthesis-specific transcripts in the cyanobacterium Synechocystis 6803, Plant Mol. Biol., 13, 693–700.

Nakao, M. *et al.* (2010). CyanoBase: the cyanobacteria genome database update 2010, Nucleic Acids Res., 38, D379–D381.

Nürnberg, D. J. *et al.* (2015). Intercellular diffusion of a fluorescent sucrose analog via the septal junctions in a filamentous cyanobacterium., mBio., 6, e02109.

Ogawa, T. *et al.* (2013). Disruption of the ndhF1 Gene Affects Chl Fluorescence through State Transition in the Cyanobacterium Synechocystis sp. PCC 6803, Resulting in Apparent High, Plant Cell Physiol., 54, 1164–1171.

Di Patti, F. *et al.* (2018). Robust stochastic Turing patterns in the development of a one-dimensional cyanobacterial organism, PLoS Biol., 16.

Petrova, O. E. *et al.* (2017). Comparative evaluation of rRNA depletion procedures for the improved analysis of bacterial biofilm and mixed pathogen culture transcriptomes., Sci. Rep., 7, 41114.

Raudvere, U. *et al.* (2019). g: Profiler: a web server for functional enrichment analysis and conversions of gene lists (2019 update), Nucleic Acids Res., 47, 191–198.

Shannon, P. *et al.* (no date). Cytoscape: A Software Environment for Integrated Models of Biomolecular Interaction Networks, genome.cshlp.org.

Stanier, R. Y. *et al.* (1979). Generic Assignments, Strain Histories and Properties of Pure Cultures of Cyanobacteria, Microbiology, 111, 1–61.

Tatusov, R. L. *et al.* (2000). The COG database: a tool for genome-scale analysis of protein functions and evolution., Nucleic Acids Res., 28, 33–6.